

BAYESIAN INFERENCE FOR SPATIAL-TEMPORAL NON-GAUSSIAN DATA USING PREDICTIVE STACKING

SOUMYAKANTI PAN^{*}, LU ZHANG[†], JONATHAN R. BRADLEY[‡], SUDIPTO BANERJEE^{*}

^{*}*Department of Biostatistics, University of California Los Angeles*

[†]*Division of Biostatistics, Department of Population and Public Health Sciences,
University of Southern California*

[‡]*Department of Statistics, Florida State University*

ABSTRACT. Analysing non-Gaussian spatial-temporal data requires introducing spatial as well as temporal dependence in generalised linear models through the link function of an exponential family distribution. Unlike in Gaussian likelihoods, inference is considerably encumbered by the inability to analytically integrate out the random effects and reduce the dimension of the parameter space. Iterative estimation algorithms struggle to converge due to the presence of weakly identified parameters. We devise Bayesian inference using predictive stacking that assimilates inference from analytically tractable conditional posterior distributions. We achieve this by expanding upon the Diaconis-Ylvisaker family of conjugate priors and exploiting generalised conjugate multivariate (GCM) distribution theory for exponential families, which enables exact sampling from analytically available posterior distributions conditional upon some process parameters. Subsequently, we assimilate inference over a range of values of these parameters using Bayesian predictive stacking. We evaluate inferential performance on simulated data, compare with full Bayesian inference using Markov chain Monte Carlo (MCMC) and apply our method to analyse spatially-temporally referenced avian count data from the North American Breeding Bird Survey database.

Keywords. Spatial GLM; model combination; Spatially-temporally varying coefficients.

1. INTRODUCTION

Statistical modelling for spatially oriented non-Gaussian outcomes plays a crucial role in various scientific applications (see, for example, [De Oliveira et al., 1997](#); [Diggle et al., 1998](#); [Heagerty and Lele, 1998](#); [De Oliveira, 2000](#); [Zhang et al., 2022](#); [Saha et al., 2022](#)). For example, climate scientists record daily or monthly binary variables at spatial locations indicating whether or not rainfall was measurable; ecologists analyse the temporal evolution of species counts at locations; and economists study the spatial distribution of the number of insurance claims over time.

For our purposes, we consider a spatial-temporal process as an uncountable set of random variables, say $\{z(\ell) : \ell \in \mathcal{D}\}$, which is endowed with a probability law specifying the joint distribution for any finite sample of locations in $\mathcal{D} \subset \mathbb{R}^d$ (with $d = 2$ or $d = 3$). In spatial-temporal settings $\mathcal{D} = \mathcal{S} \times \mathcal{T}$, where $\mathcal{S} \subset \mathbb{R}^d$ and $\mathcal{T} \subset [0, \infty)$ are space and time domains, respectively, and $\ell = (s, t)$ is a space-time coordinate with $s \in \mathcal{S}$ and $t \in \mathcal{T}$ (see, e.g., [Gneiting and Guttorp, 2010](#)).

Date: December 29, 2025.

Following [Diggle et al. \(1998\)](#), we introduce a spatial-temporal stochastic processes for non-Gaussian data. Let $y(\ell)$ be the outcome at ℓ endowed with a probability law from the natural exponential family, which we denote by

$$y(\ell) \sim \text{EF}(x(\ell)^\top \beta + z(\ell); b, \psi_y) \quad (1)$$

for some positive parameter $b > 0$ and the unit log partition function ψ_y ([Section 2.1](#)). Fixed effects and spatial dependence, e.g., $x(\ell)^\top \beta + z(\ell)$, are introduced in the natural parameter, where $x(\ell)$ is a $p \times 1$ vector of predictors referenced with respect to ℓ , β is a $p \times 1$ vector of slopes, $z(\ell)$ is a zero-centred spatial-temporal Gaussian process on \mathbb{R}^d specified by a scale parameter σ_z and a spatial-temporal correlation function $R(\cdot, \cdot; \theta_{\text{sp}})$ with θ_{sp} consisting of spatial-temporal decay and smoothness parameters. This structure is embodied by spatial-temporal generalised mixed-effect models ([McCulloch and Searle, 2001](#); [Hughes and Haran, 2013](#)). Bayesian inference for [\(1\)](#) is appealing as it offers fully probabilistic inference for the latent process. However, the presence of $z(\ell)$ presents challenges for non-Gaussian families as we cannot integrate out z , which begets a high-dimensional parameter space. Iterative algorithms such as Markov Chain Monte Carlo (MCMC) attempt to sample from the posterior distribution, but are often encumbered by high auto-correlations and weakly identified parameters θ_{sp} . [Section 1.3](#) in [Haran \(2011\)](#) overviews MCMC algorithms for estimating such models.

This article departs from the customary focus on improving computational algorithms for spatial generalised linear models (GLMs). Instead, we devise Bayesian predictive stacking to conduct Bayesian inference for fixed effects and the latent spatial-temporal process by avoiding MCMC or other iterative algorithms for spatial-temporal non-Gaussian data. Stacking ([Wolpert, 1992](#); [Breiman, 1996](#); [Clyde and Iversen, 2013](#)) is a model averaging procedure that is widely used in machine learning and has been shown (see, e.g., [Le and Clarke, 2017](#); [Yao et al., 2018, 2022, 2021](#); [Zhang et al., 2025](#)) to be an effective alternative to traditional Bayesian model averaging ([Madigan et al., 1996](#); [Hoeting et al., 1999](#)). We divide our model parameters into two sets $\theta_1 = \{\beta, z, \sigma\}$ and $\theta_2 = \{\theta_{\text{sp}}, \cdot\}$, where σ denotes a collection of scale parameters associated with β and z , and \cdot represents other auxiliary model parameters. We use conjugate distribution theory so that $p(\theta_1 | y, \theta_2)$ is available in closed form. We are primarily concerned with Bayesian inference on θ_1 averaging out θ_2 . Therefore, our desired posterior distribution is $p(\theta_1 | y) = \int p(\theta_1 | y, \theta_2) p(\theta_2 | y) d\theta_2$. The key bottleneck here is that $p(\theta_2 | y)$ is intractable. This further precludes empirical Bayes strategies, as evaluating $p(\theta_2 | y)$ requires marginalization over θ_1 , which entails a high-dimensional numerical integration and is itself computationally expensive. Therefore, we reformulate our inference problem by writing $p(\theta_1 | y) = \int p(\theta_1 | y, \theta_2) p(\theta_2 | y) d\theta_2 \approx \sum_{g=1}^G w_g p(\theta_1 | y, \theta_{2g})$, where the collection of weights w_g replaces $p(\theta_2 | y)$. A key distinction from quadrature based methods (e.g., INLA, [Rue et al., 2009](#)) is that we do not attempt to approximate $p(\theta_2 | y)$. Instead, we find w_g using convex optimisation with scoring rules. Once the optimal weights, say \hat{w}_g , are computed, posterior inference for quantities of interest proceeds from the ‘‘stacked posterior’’ $\tilde{p}(\cdot | y) = \sum_{g=1}^G \hat{w}_g p(\cdot | y, \theta_{2g})$.

We develop and investigate Bayesian predictive stacking for spatial-temporal GLMs (thereby extending [Zhang et al., 2025](#), to spatial-temporal non-Gaussian data). This requires hierarchical models to produce analytically accessible posterior distributions for θ_1 subject to fixing weakly

identified parameters θ_2 and some hyperparameters to draw exact posterior samples for any fixed values of these parameters. Here, we avail of a new class of analytically accessible generalised conjugate multivariate distributions (GCM) for spatial models (Bradley and Clinch, 2024) by extending the Diaconis-Ylvisaker family of conjugate priors for exponential families (Diaconis and Ylvisaker, 1979). We significantly expand on this framework by considering spatial-temporal processes and further enrich (1) by introducing spatially-temporally varying regression coefficients (Gelfand et al., 2003) to capture the impact of predictors over space and time. Bayesian modelling is especially appealing here, as it offers inference on processes that are completely unobserved.

The literature on spatially-temporally varying coefficient models is rather sparse and has remained purely notional for exponential families, perhaps because they require extensive tuning of MCMC or other iterative algorithms that struggle with weakly identified parameters and high-dimensional random effects. Our subsequent development offers, as we demonstrate below, a fast and effective inferential tool for analysing spatial-temporal count or binary data. The analytical tractability we seek will forego inference on some weakly identifiable parameters (θ_2 above), but the key inferential objectives concerning the natural mean function (e.g., regression coefficients), the spatial-temporal process and the variance components are retained. We show that the inference obtained on these parameters is practically indistinguishable from full inference using MCMC.

After briefly discussing some necessary distributions in Section 2, Section 3 introduces our hierarchical spatially-temporally varying regression model and derives analytical posterior distributions. Section 4 develops predictive stacking with novel results on posterior sampling and predictive inference. Sections 5 and 6 present simulation experiments demonstrating the effectiveness of our method and analyse a spatial-temporal bird counts data. Section 7 concludes with a brief discussion.

2. CONJUGATE PRIORS FOR EXPONENTIAL FAMILY

2.1. The Diaconis-Ylvisaker distribution. Let Y be distributed from the natural exponential family, $\text{EF}(\eta; b, \psi)$, with density

$$p(Y | \eta) = \exp\{\eta Y - b\psi(\eta) + c(Y)\}, \quad Y \in \mathcal{Y}, \eta \in \mathcal{H}, \quad (2)$$

where \mathcal{Y} denotes the support of Y and $\mathcal{H} = \{\eta : \psi(\eta) < \infty\}$ denotes the natural parameter space and, therefore, the support of η . The scalar b may be unknown, while $\psi(\cdot)$ and $c(\cdot)$ are known functions. We will discuss various forms of the unit log partition function $\psi(\cdot)$ and the scalar b to denote different distributions of the family. For example, $\psi_1(t) = t^2$ with $b = 1/2\sigma^2$, $\psi_2(t) = e^t$ with $b = 1$ and $\psi_3(t) = \log(1 + e^t)$ with $b = 1$ or $m > 1$ correspond to the Gaussian with variance σ^2 , Poisson, binary or binomial distributions, respectively.

Diaconis and Ylvisaker (1979) proposes a proper conjugate prior for η in (2),

$$p(\eta | \alpha, \kappa) \propto \exp\{\alpha\eta - \kappa\psi(\eta)\}, \quad \eta \in \frac{\alpha}{\kappa} \in \mathcal{Y}, \kappa > 0, \quad (3)$$

which we denote as $\eta \sim \text{DY}(\alpha, \kappa; \psi)$. It follows that $\eta | Y, \alpha, \kappa \sim \text{DY}(\alpha + Y, \kappa + b; \psi)$. Special cases of the DY distribution include Gaussian ($\psi = \psi_1$), log-gamma ($\psi = \psi_2$), and logit-beta ($\psi = \psi_3$). Some may not belong to the exponential family. For example, $\alpha = 0$, $\psi(t) = \psi_4(t, \nu) = \log(1 + t^2/\nu)$, and $\kappa = (\nu + 1)/2$ with $\nu > 0$ yield a Student's t -distribution with ν degrees of freedom.

2.2. The Generalised Conjugate Multivariate distribution. We modify the generalised conjugate multivariate random variable (GCM) introduced by [Bradley and Clinch \(2024\)](#) using linear combinations of mutually independent DY random variables. We define ζ as the $n \times 1$ random vector

$$\zeta = \mu + LD(\theta)\eta, \quad (4)$$

where the location parameter μ is $n \times 1$, $\eta = (\eta_1, \dots, \eta_n)^\top$ with elements $\eta_i \stackrel{\text{ind}}{\sim} \text{DY}(\alpha_i, \kappa_i; \psi_i)$ with $\kappa_i > 0$ for $i = 1, \dots, n$, L is $n \times n$ lower-triangular with positive diagonal elements, θ denotes a set of scale parameters with parameter space Θ , and $D(\theta)$ is an $n \times n$ invertible matrix for all values of $\theta \in \Theta$. Given θ , we use (3) to derive the conditional density of ζ up to a proportionality constant,

$$p(\zeta \mid \mu, L, \theta, \alpha, \kappa; \psi) \propto \exp \left\{ \alpha^\top D(\theta)^{-1} L^{-1} (\zeta - \mu) - \kappa^\top \psi (D(\theta)^{-1} L^{-1} (\zeta - \mu)) \right\} \det(L^{-1}) \det(D(\theta)^{-1}), \quad (5)$$

where $\psi = (\psi_1, \dots, \psi_n)^\top$, and $\psi(D(\theta)^{-1} L^{-1} (\zeta - \mu))$ is an $n \times 1$ vector with its i th element $\psi_i(e_i^\top D(\theta)^{-1} L^{-1} (\zeta - \mu))$, e_i is the vector of zeros with 1 at the i th position, $\alpha = (\alpha_1, \dots, \alpha_n)^\top$ and $\kappa = (\kappa_1, \dots, \kappa_n)^\top$ are $n \times 1$ shape and scale parameters. The GCM is derived from (5) considering a probability law for θ independent of the remaining parameters, i.e., $\pi(\theta) := \pi(\theta \mid \mu, L, \alpha, \kappa)$. We write $\zeta \sim \text{GCM}(\mu, L, \alpha, \kappa, D, \pi; \psi)$ to denote $p(\zeta \mid \mu, L, \alpha, \kappa; \psi) \propto \mathbb{E}_\theta [p(\zeta \mid \mu, L, \theta, \alpha, \kappa; \psi)]$.

Moreover, suppose $\zeta = (\zeta_1^\top, \zeta_2^\top)^\top$, where ζ_1 is $r \times 1$ and ζ_2 is $(n - r) \times 1$. Then, given θ , the conditional density of ζ_1 given ζ_2 up to a proportionality constant is

$$p(\zeta_1 \mid \zeta_2 = c_2, \mu^*, A_1, \theta, \alpha, \kappa; \psi) \propto \exp \left\{ \alpha^\top (D(\theta)^{-1} A_1 \zeta_1 - \mu^*) - \kappa^\top \psi (D(\theta)^{-1} A_1 \zeta_1 - \mu^*) \right\} \det(D(\theta)^{-1}), \quad (6)$$

where A_1 is the $n \times r$ submatrix of $L^{-1} = [A_1, A_2]$, and $\mu^* = D(\theta)^{-1} L^{-1} \mu - D(\theta)^{-1} A_2 c_2$ for some $c_2 \in \mathbb{R}^{n-r}$. The proportionality constant in (6) is strictly positive and finite, ensuring that (6) is proper ([Bradley et al., 2020](#)). Under the same assumptions of $\pi(\theta)$ as above, we write $\zeta_1 \mid \zeta_2 \sim \text{GCM}_c(\mu^*, A_1, \alpha, \kappa, D, \pi; \psi)$ for $p(\zeta_1 \mid \zeta_2, \mu, L, \alpha, \kappa; \psi) \propto \mathbb{E}_{\theta \mid \zeta_2, \mu, L, \alpha, \kappa; \psi} [p(\zeta_1 \mid \zeta_2, \mu, L, \theta, \alpha, \kappa; \psi)]$.

We use these distributions to build hierarchical models in the following sections. In general, we may be unable to sample directly from the conditional GCM distribution except for some familiar exceptions (e.g., the conditional distribution of Gaussian is indeed Gaussian). However, it is possible to consider an augmented model with a particular structure that yields a posterior distribution in the GCM family that is easy to sample from (Section 3).

3. BAYESIAN HIERARCHICAL MODEL

3.1. Conjugate Bayesian spatially-temporally varying coefficients model. Let $\mathcal{L} = \{\ell_1, \dots, \ell_n\}$ be a fixed set of n distinct space-time coordinates in \mathcal{D} , where $y(\mathcal{L}) = (y(\ell_1), \dots, y(\ell_n))^\top \in \mathcal{Y}^n$, which we simply denote by y , is the vector of observed outcomes, each distributed as a member of the natural exponential family with log partition function ψ_y . Suppose, $x(\ell_i)$ is a $p \times 1$ vector of predictors, β is the corresponding $p \times 1$ vector of slopes (fixed effects), $\tilde{x}(\ell_i)$ is $r \times 1$ ($r \leq p$) consisting of predictors in $x(\ell_i)$ that are posited to have spatially-temporally varying regression coefficients $z(\ell_i) = (z_1(\ell_i), \dots, z_r(\ell_i))^\top$, where each $z_j(\ell_i)$ is a spatially-temporally varying coefficient for the

predictor $\tilde{x}_j(\ell_i)$, ξ_i is a fine-scale variation term and μ_i is the discrepancy parameter (Bradley et al., 2020). We introduce spatially-temporally varying coefficients in $\eta(\ell)$ as

$$\begin{aligned}
y(\ell_i) \mid \beta, z(\ell_i), \xi_i, \mu_i &\stackrel{\text{ind}}{\sim} \mathbf{EF}(\eta(\ell_i) + \xi_i - \mu_i; b_i, \psi_y), \quad i = 1, \dots, n, \\
\eta(\ell) &= x(\ell)^\top \beta + \tilde{x}(\ell)^\top z(\ell), \quad \beta \mid \sigma_\beta^2, \mu_\beta, V_\beta \sim \mathbf{N}(\mu_\beta, \sigma_\beta^2 V_\beta), \quad \sigma_\beta^2 \sim \pi_\beta(\sigma_\beta^2), \\
z(\ell) \mid \theta_z, \theta_{\text{sp}} &\sim \mathcal{GP}(0, C_z(\cdot, \cdot; \theta_{\text{sp}}, \theta_z)), \quad \theta_z \sim \pi_z(\theta_z), \\
\xi \mid \beta, z, \mu, \alpha_\epsilon, \kappa_\epsilon, \sigma_\xi^2 &\sim \mathbf{GCM}_c(\tilde{\mu}_\xi, H_\xi, \alpha_\xi, \kappa_\xi, D_\xi, \pi_\xi; \psi_\xi), \quad \sigma_\xi^2 \sim \pi_\xi(\sigma_\xi^2), \quad p(\mu) \propto 1,
\end{aligned} \tag{7}$$

where $z(\ell) = (z_1(\ell), \dots, z_r(\ell))^\top$ is a multivariate Gaussian process with a separable cross-covariance function $C_z(\cdot, \cdot; \theta_{\text{sp}}, \theta_z)$, characterised by the process parameters θ_{sp} that control the spatial-temporal correlation within the process and θ_z that control the covariance matrix between the processes (Mardia and Goodall, 1993). Given θ_z , the $nr \times 1$ vector $z = (z_1^\top, \dots, z_r^\top)^\top$, where $z_j = (z_j(\ell_1), \dots, z_j(\ell_n))^\top$ for $j = 1, \dots, r$, follows a multivariate Gaussian distribution with mean 0 and $nr \times nr$ covariance matrix $C_z(\mathcal{L}; \theta_{\text{sp}}, \theta_z)$. We discuss different specifications for C_z in Section 3.3.

Let X be $n \times p$ with the value of the j th predictor at ℓ_i as the (i, j) -th element $x_j(\ell_i)$ for $j = 1, \dots, p$, and $\tilde{X} = [\text{diag}(\tilde{x}_1), \dots, \text{diag}(\tilde{x}_r)]$ is $n \times nr$ with $\text{diag}(\tilde{x}_j)$ being an $n \times n$ diagonal matrix whose i th diagonal element is $\tilde{x}_j(\ell_i)$ for $j = 1, \dots, r$. The conditional prior for ξ is characterised by the $2n \times 1$ location $\tilde{\mu}_\xi = ((\mu - X\beta - \tilde{X}z)^\top, 0_n^\top)^\top$, where 0_k denotes the vector of zeros of length $k \in \mathbb{N}$, $2n \times n$ matrix $H_\xi = [I_n, I_n]^\top$, $2n \times 2n$ block-diagonal matrix $D_\xi(\sigma_\xi^2) = \text{blkdiag}(I_n, \sigma_\xi^2 I_n)$. The shape parameter $\alpha_\xi = (\alpha_\epsilon 1_n^\top, 0_n^\top)^\top$ and the scale parameter $\kappa_\xi = (\kappa_\epsilon 1_n^\top, (1/2)1_n^\top)^\top$, where 1_k is the vector of ones of length $k \in \mathbb{N}$. Finally, we assume $p(\mu) \propto 1$.

Instead of applying MCMC to sample from (7), we devise predictive stacking that averages over models specified by fixing parameters and hyperparameters that serve to tune inference but are not, by themselves, of interest. Therefore, let M denote a generic version of (7) obtained by specifying fixed values for θ_{sp} , the boundary adjustment parameters $\{\alpha_\epsilon, \kappa_\epsilon\}$, hyperparameters μ_β, V_β and other auxiliary hyperparameters present in the hyperprior $\pi(\theta) = \pi_z(\theta_z) \pi_\beta(\sigma_\beta^2) \pi(\sigma_\xi^2)$ for $\theta = \{\theta_z, \sigma_\beta^2, \sigma_\xi^2\}$. These specifications ensure analytically accessible posterior distributions from the GCM family that are easy to sample from. The model in (7) collapses into a parsimonious representation by integrating out the scale parameters θ with respect to the prior $\pi(\theta)$. This yields

$$\begin{aligned}
y(\ell_i) \mid \beta, z(\ell_i), \xi_i, \mu_i &\stackrel{\text{ind}}{\sim} \mathbf{EF}(\eta(\ell_i) + \xi_i - \mu_i; b_i, \psi_y), \quad i = 1, \dots, n \\
(\gamma^\top, q^\top)^\top \mid M &\sim \mathbf{GCM}(0_{2n+p+nr}, V, \alpha, \kappa, D, \pi; \psi),
\end{aligned} \tag{8}$$

where $\gamma = (\xi^\top, \beta^\top, z^\top)^\top$, with $n \times 1$ vector $\xi = (\xi_1, \dots, \xi_n)^\top$ and q is a reparametrization of μ , which we detail below. The matrix V is $(2n + p + nr) \times (2n + p + nr)$ such that $V^{-1} = [H, Q]$, where

$$H = \begin{bmatrix} I_n & X & \tilde{X} \\ I_n & 0 & 0 \\ 0 & L_\beta^{-1} & 0 \\ 0 & 0 & L_z^{-1} \end{bmatrix} \text{ is } (2n + p + nr) \times (n + p + nr) \text{ and } Q \text{ is } (2n + p + nr) \times n \text{ whose columns are}$$

the n orthonormal eigenvectors of $I - P_H$ corresponding to eigenvalue 1 with $P_H = H(H^\top H)^{-1}H^\top$ being the orthogonal projection matrix on the column space of H , L_β is the lower-triangular

Cholesky factor of V_β and L_z is an $nr \times nr$ lower-triangular matrix obtained from our specification of $C_z(\mathcal{L}; \theta_{\text{sp}}, \theta_z)$ (see Section 3.3 for details on L_z).

We define $q = -Q^T D(\theta) \tilde{\mu}$, where $\tilde{\mu} = (\mu^T, 0_n^T, \mu_\beta^T L_\beta^{-T}, 0_{nr}^T)^T$ and $\mu = (\mu_1, \dots, \mu_n)^T$. Here, $D(\theta) = \text{blkdiag}(I_n, \sigma_\xi I_n, \sigma_\beta I_p, D_z(\theta_z))$. Finally, the shape and scale parameters of GCM in (8) are $\alpha = (\alpha_\epsilon 1_n^T, 0_{n+p+nr}^T)^T$, and, $\kappa = (\kappa_\epsilon 1_n^T, (1/2)1_{n+p+nr}^T)^T$. The unit log partition function $\psi(\cdot)$ in (8) is $\psi(h) = (\psi_y(h_1)^T, \psi_1(h_2)^T)^T$ for some $h = (h_1^T, h_2^T)^T$ with $h_1 \in \mathbb{R}^n$, $h_2 \in \mathbb{R}^{n+p+nr}$, where all log partition functions operate element-wise on the arguments. See Lemma A1 and Theorem A1 in Appendix A for technical details.

3.2. Posterior distribution. The hierarchical model (7) (or (8)) yields the posterior distribution

$$(\gamma^T, q^T)^T \mid y, M \sim \text{GCM}(0_{2n+p+nr}, V, \alpha^*, \kappa^*, D, \pi; \psi), \quad (9)$$

where the shape and scale parameters are $\alpha_* = ((y + \alpha_\epsilon 1_n)^T, 0_{n+p+nr}^T)^T$ and $\kappa_* = ((b + \kappa_\epsilon 1_n)^T, (1/2)1_{n+p+nr}^T)^T$ (Theorem A2 in Appendix A). Generalised linear models typically assume μ (and hence q) to be zero. This yields $p(\gamma \mid y, M)$ to be a GCM_c distribution, which we cannot sample directly from, except for some special cases of ψ_y (e.g., Gaussian). We note that μ is crucial in producing the posterior distribution within the GCM family and therefore, unlike traditional generalised linear models, cannot be excluded from (7). Parameters $\{\alpha_\epsilon, \kappa_\epsilon\}$ ensure that the posterior shape and scale parameters α^* and κ^* do not lie on the boundary of the parameter space, and hence the inclusion of ξ is necessary for a well-defined posterior distribution.

3.3. Fixed effects and spatial-temporal processes. In practice, we have found σ_ξ^2 to have little impact on posterior inference and therefore fix it to a small positive number, i.e., $\pi(\sigma_\xi^2) = \delta_c$ for some $c > 0$, where δ_c corresponds to the Dirac measure on a real c . We also assign an inverse-gamma prior $\pi(\sigma_\beta^2) = \text{IG}(\sigma_\beta^2 \mid \nu_\beta/2, \nu_\beta/2)$. Similarly, we model z using a spatial-temporal Gaussian process, and subsequently place the inverse-gamma/inverse-Wishart prior on the scale parameter θ_z . Below, we discuss some possible spatial-temporal process models to study the spatially-temporally varying effects of the predictors on the response.

3.3.1. Independent spatial-temporal processes. We consider r independent Gaussian spatial-temporal processes

$$\begin{aligned} \text{Independent processes: } z_j(\ell) \mid \sigma_{z_j}^2, \theta_{\text{sp}j} &\stackrel{\text{ind}}{\sim} \mathcal{GP}(0, \sigma_{z_j}^2 R_j(\cdot, \cdot; \theta_{\text{sp}j})), \\ \sigma_{z_j}^2 &\sim \text{IG}(\nu_{z_j}/2, \nu_{z_j}/2), \quad j = 1, \dots, r, \end{aligned} \quad (10)$$

where $\sigma_{z_j}^2$ is the variance parameter corresponding to the process $z_j(\ell)$. This corresponds to the covariance matrix $C_z(\mathcal{L}; \theta_{\text{sp}}, \theta_z) = \bigoplus_{j=1}^r \sigma_{z_j}^2 R_j(\theta_{\text{sp}j})$ in (7) with $\theta_{\text{sp}} = \{\theta_{\text{sp}j} : j = 1, \dots, r\}$, where $\theta_{\text{sp}j}$ denotes the covariance kernel parameters for the j th process and $\theta_z = \{\sigma_{z_1}^2, \dots, \sigma_{z_r}^2\}$. We let L_z be the $nr \times nr$ lower-triangular Cholesky factor of the block diagonal matrix $\bigoplus_{j=1}^r R_j(\theta_{\text{sp}j})$ and $D_z(\theta_z) = \bigoplus_{j=1}^r \sigma_{z_j} I_n$, such that $C_z(\mathcal{L}; \theta_{\text{sp}}, \theta_z) = L_z D_z D_z^T L_z^T$. Lastly, (10) places independent inverse-gamma priors on each scale parameter, given by $\pi(\theta_z) = \prod_{j=1}^r \text{IG}(\sigma_{z_j}^2 \mid \nu_{z_j}/2, \nu_{z_j}/2)$.

3.3.2. *Multivariate spatial-temporal process.* We can introduce dependence among the elements of the $r \times 1$ vector $z(\ell)$ using

$$\text{Multivariate process: } z(\ell) \mid \Sigma \sim \mathcal{GP}(0, R(\cdot, \cdot; \theta_{\text{sp}})\Sigma), \quad \Sigma \sim \text{IW}(\nu_z + 2r, \Psi), \quad (11)$$

where $\mathcal{GP}(0, R(\cdot, \cdot; \theta_{\text{sp}})\Sigma)$ is an $r \times 1$ multivariate Gaussian process with matrix-valued cross-covariance function $R(\cdot, \cdot; \theta_{\text{sp}})\Sigma$ and Σ is an $r \times r$ positive definite random matrix. This corresponds to the spatial-temporal covariance matrix $C_z(\mathcal{L}; \theta_{\text{sp}}, \theta_z) = \Sigma \otimes R(\theta_{\text{sp}})$ in (7) with $\theta_z = \Sigma$. Here, we let L_z be the $nr \times nr$ lower-triangular Cholesky factor of the block-diagonal matrix $I_r \otimes R(\theta_{\text{sp}})$ and $D_z(\theta_z) = \Sigma^{1/2} \otimes I_n$, where \otimes denotes the Kronecker product. Hence, given Σ , the $n \times r$ matrix $Z = [z_1 : \dots : z_r]$ follows a matrix normal distribution $\text{MN}_{n,r}(0, R(\theta_{\text{sp}}), \Sigma)$ (Gupta and Nagar, 1999, Chapter 2.2). We place an inverse-Wishart prior on the scale parameter with the shape $\nu_z + 2r$ and $r \times r$ positive definite scale matrix Ψ (see, e.g., Gupta and Nagar, 1999, Chapter 3.4), given by $\pi(\theta_z) = \text{IW}(\Sigma \mid \nu_z + 2r, \Psi)$.

3.3.3. *Spatial-temporal correlation kernel.* For independent processes, elements of $R_j(\theta_{\text{sp}_j})$ are evaluated using a spatial-temporal correlation function (see, e.g., Gneiting and Guttorp, 2010)

$$R_j(\ell, \ell'; \theta_{\text{sp}_j}) = \frac{1}{\phi_{1j}|t - t'|^2 + 1} \exp\left(-\frac{\phi_{2j}\|s - s'\|}{\sqrt{1 + \phi_{1j}|t - t'|^2}}\right), \quad \phi_{1j}, \phi_{2j} > 0, \quad (12)$$

where $\ell = (s, t)$ and $\ell' = (s', t')$ are any two distinct space-time coordinates in \mathcal{D} , $\|\cdot\|$ is the Euclidean distance over \mathcal{S} , $\theta_{\text{sp}_j} = (\phi_{1j}, \phi_{2j})$, and ϕ_{1j} and ϕ_{2j} are positive spatial and temporal decay parameters, respectively. We gather the $2r$ process parameters in $\theta_{\text{sp}} = \{\theta_{\text{sp}_j} : j = 1, \dots, r\}$. For ease of notation, we drop θ_{sp_j} and simply write $R_j(\cdot, \cdot)$ for the correlation function. For the multivariate model in (11), $R(\cdot, \cdot; \theta_{\text{sp}})$ corresponds to (12) with $\theta_{\text{sp}} = \{\phi_1, \phi_2\}$.

4. PREDICTIVE STACKING

4.1. **Choice of candidate models.** We consider modelling data typically originating from Poisson ($\psi_y = \psi_2$), binomial and binary ($\psi_y = \psi_3$) distributions. In order to implement stacking, we first fix values of certain hyperparameters. In practice, we assume $\mu_\beta = 0$, $V_\beta = \delta_\beta^2 I_p$ for some real δ_β , and some $\nu_\beta > 2$ to specify the priors of fixed effects β and σ_β^2 . Moreover, under the assumption of independent processes, we assume $\nu_{z_j} > 2$ for each j , and, on the other hand, $\nu_z > 2$ and some positive definite Ψ for the assumption of a multivariate process on varying coefficients.

Once the hyperparameters are fixed, we consider a grid of candidate values for the spatial process parameters θ_{sp} and the boundary adjustment parameter α_ϵ , conditional on which we sample from the posterior (9). We choose $\alpha_\epsilon > 0$ in the prior of ξ to ensure that α^* in (9) does not lie on the boundary of its parameter space. For Poisson data, $\kappa_\epsilon = 0$ and for binary/binomial data, $\kappa_\epsilon = 2\alpha_\epsilon$. A natural approach to construct a collection of candidate models \mathcal{M} is to consider a Cartesian product of candidate values for each parameter in $\{\theta_{\text{sp}}, \alpha_\epsilon\}$. Although that is computationally viable under the multivariate specification (11), where $\theta_{\text{sp}} = \{\phi_1, \phi_2\}$ is of a lower dimension compared to that of independent processes (10), where $\theta_{\text{sp}} = \{(\phi_{1j}, \phi_{2j}) : j = 1, \dots, r\}$ is $2r$ -dimensional. In the latter case, the number of models, when naively constructed, grows exponentially, undermining the computational advantage gained by sampling from analytically available posterior distributions.

Instead, in this case, we build \mathcal{M} using a fixed number of random candidate values of θ_{sp} , sampled uniformly from a $2r$ -dimensional rectangle specified by plausible lower and upper bounds for each parameter, likely supplied by the user.

4.2. Sampling from posterior. Sampling from the posterior distribution (9) proceeds by first sampling replicates from the family of marginal priors for γ obtained by integrating out the scale parameters. We elaborate in the following. Since $[H, Q]^{-1} = [H(H^T H)^{-1}, Q]^T$, we compute

$$\gamma^{(b)} = (H^T H)^{-1} H^T v^{(b)} \quad \text{and} \quad q^{(b)} = Q^T v^{(b)} \quad (13)$$

to obtain $(\gamma^{(b)T}, q^{(b)T})^T$, $b = 1, \dots, B$ of $(\gamma^T, q^T)^T$, where $v^{(b)}$ is a sample from the distribution $\text{GCM}(0, I_{2n+p+nr}, \alpha^*, \kappa^*, D, \pi; \psi_\gamma)$. The random vector $v^{(b)} = (v_\eta^{(b)T}, v_\xi^{(b)T}, v_\beta^{(b)T}, v_z^{(b)T})^T$ is made up of $v_\eta^{(b)}$, where $v_{\eta,i}^{(b)} \sim \text{DY}(y_i + \alpha_\epsilon, b + \kappa_\epsilon; \psi_y)$ for $i = 1, \dots, n$ and $v_\beta^{(b)}, v_z^{(b)} = (v_{z_1}^{(b)}, \dots, v_{z_r}^{(b)})^T$, and $v_\xi^{(b)}$ is a sample from $\text{N}(0, \sigma_\xi^2 I_n)$ for each b . The $n \times 1$ random vector $v_\eta^{(b)}$ has its i -th element as $\eta^{(b)}(\ell_i) + \xi_i^{(b)} - \mu_i^{(b)}$.

The projection in (13) maps the posterior samples of η to the posterior samples of γ accounting for the effect of its priors. It is instructive to rewrite (13) as

$$\gamma^{(b)} = (H_1^T H_1 + V_\gamma^{-1})^{-1} (H_1^T v_\eta^{(b)} + L_\gamma^{-T} v_\gamma^{(b)}), \quad (14)$$

where $H = [H_1^T, L_\gamma^{-T}]^T$ with $H_1 = [I_n, X, \tilde{X}]$, $V_\gamma = L_\gamma L_\gamma^T$, and $v_\gamma^{(b)} = (v_\xi^{(b)T}, v_\beta^{(b)T}, v_z^{(b)T})^T$. We leverage the structure of H and the sparsity of \tilde{X} to achieve a computationally efficient algorithm for evaluating (14). Section B.1 of the Appendix summarises an optimised algorithm for computing (14) given a $v^{(b)}$. Moreover, the posterior samples of the scale parameters are recovered from the posterior samples of $\{\beta^{(b)}, z^{(b)}\}$ from the marginal model (Section A.5 in the Appendix).

Posterior predictive inference for the spatial-temporal process is carried over to the canonical mean $\eta(\ell) = x(\ell)^T \beta + \tilde{x}(\ell)^T z(\ell)$. For each value of $\{\beta^{(b)}, z^{(b)}(\ell)\}$ drawn from the posterior distribution (9), we obtain the corresponding sample $\eta^{(b)}(\ell) = x(\ell)^T \beta^{(b)} + \tilde{x}(\ell)^T z^{(b)}(\ell)$. This can be achieved at any arbitrary space-time coordinate ℓ . If $\ell \in \mathcal{L}$, then we can further generate model replicated data $Y_{\text{rep}}^{(b)}(\ell_i) \sim \text{EF}(\eta^{(b)}(\ell_i) + \xi_i^{(b)} - \mu_i^{(b)}; b_i, \psi_y)$ for each posterior draw of $\{\eta^{(b)}(\ell_i), \xi_i^{(b)}, \mu_i^{(b)}\}$. If, on the other hand, $\ell \notin \mathcal{L}$, then we seek predictive inference. Here, we can still carry out inference for $\eta(\ell)$ but cannot coherently extend inference to the outcome $Y(\ell)$. This is an artefact of spatial GLMs, where the well-defined process $z(\ell)$ in $\eta(\ell)$ does not extend to the outcome. Although we have a well-defined joint distribution for outcomes on a finite set of points, we do not have a corresponding stochastic process $Y(\ell)$ across the domain (Banerjee et al., 2025). Section 4.3 offers posterior predictive inference by defining predictive random variables $\tilde{Y}(\tilde{\ell}) \sim \text{EF}(\eta(\tilde{\ell}); \tilde{b}, \psi_y)$.

4.3. Spatial-temporal prediction. Given the data observed at \mathcal{L} , let $\tilde{\mathcal{L}} = \{\tilde{\ell}_1, \dots, \tilde{\ell}_{\tilde{n}}\} \subset \mathcal{D} \setminus \mathcal{L}$ be a collection of \tilde{n} new space-time coordinates in \mathcal{D} , where we wish to predict the response and the latent spatial-temporal processes. Let \tilde{y} and \tilde{z}_j for each j be the $\tilde{n} \times 1$ vectors with the i th elements $y(\tilde{\ell}_i)$ and $z_j(\tilde{\ell}_i)$, respectively. For a given model, M , which entails a fixed value of θ_{sp} and some auxiliary model parameters, spatial-temporal predictive inference evaluates the posterior

predictive distribution,

$$p(\tilde{y}, \tilde{z} \mid y, M) = \int p(\tilde{y} \mid \beta, \tilde{z})p(\tilde{z} \mid z, M)p(\beta, z \mid y, M)d\beta dz, \quad (15)$$

where $\tilde{z} = (\tilde{z}_1^T, \dots, \tilde{z}_r^T)^T$. We sample from (15) first drawing $\{\beta^{(b)}, z^{(b)}\}$ from $p(\beta, z \mid y, M)$ as described in Section 4.2 and then, for each drawn value $z^{(b)}$ from z , drawing $\tilde{z}^{(b)}$ from $p(\tilde{z} \mid z, M)$. Furthermore, for each posterior sample $\beta^{(b)}$ and $\tilde{z}^{(b)}$, we draw $\tilde{y}^{(b)}$ from $p(\tilde{y} \mid \beta, \tilde{z})$ with μ in (7) set to 0. This yields $\{\tilde{y}^{(b)}, \tilde{z}^{(b)}\}$ from (15).

For the independent process model in (10), the marginal distribution of the $(n + \tilde{n}) \times 1$ vector $(z_j^T, \tilde{z}_j^T)^T$ corresponding to the j th process is a multivariate t -distribution $t_{n+\tilde{n}}(\nu_{z_j}, 0_n, \tilde{V}_{z_j})$ with ν_{z_j} degrees of freedom, location parameter 0_n and $(n + \tilde{n}) \times (n + \tilde{n})$ scale matrix $\tilde{V}_z = \begin{bmatrix} R_j & C_j \\ C_j^T & \tilde{R}_j \end{bmatrix}$, where \tilde{R}_j is the $\tilde{n} \times \tilde{n}$ correlation matrix for \tilde{z}_j , and $C_j = [R_j(\ell, \ell')]$ is $n \times \tilde{n}$ with $\ell \in \mathcal{L}, \ell' \in \tilde{\mathcal{L}}$. This yields

$$\tilde{z}_j \mid z_j, M \sim t_{\tilde{n}} \left(\nu_{z_j} + n, C_j^T R_j^{-1} z_j, \frac{\nu_{z_j} + z_j^T R_j^{-1} z_j}{\nu_{z_j} + n} (\tilde{R}_j - C_j^T R_j^{-1} C_j) \right), \quad (16)$$

for $j = 1, \dots, r$. It should be noted that the conditional scale matrix contains the factor $(\nu_{z_j} + z_j^T R_j^{-1} z_j)/(\nu_{z_j} + n)$ which is directly related to the Mahalanobis distance of z_j , implying that the dispersion is enlarged in the presence of extreme values of z_j . The degrees of freedom also increase by a factor n , which means that the more data we have, the less heavy-tailed $p(\tilde{z}_j \mid z_j, M)$ becomes (Ding, 2016).

For the multivariate process in (11), the marginal distribution of the $(n + \tilde{n}) \times r$ random matrix $[Z^T, \tilde{Z}^T]^T$, where $\tilde{Z} = [\tilde{z}_1, \dots, \tilde{z}_r]$ follows a matrix t -distribution $\text{MT}_{n+\tilde{n}, r}(\nu_z, 0, \tilde{V}_z, \Psi)$ with $(n + \tilde{n}) \times (n + \tilde{n})$ matrix $\tilde{V}_z = \begin{bmatrix} R & C \\ C^T & \tilde{R} \end{bmatrix}$ defined accordingly (R, C and \tilde{R} are common across j). We derive $p(\tilde{Z} \mid Z, M)$ as

$$\tilde{Z} \mid Z, M \sim \text{MT}_{\tilde{n}, r} \left(\nu_z + n, C^T R^{-1} Z, \tilde{R} - C^T R^{-1} C, \Psi + Z^T R^{-1} Z \right). \quad (17)$$

For technical details, see Theorem A.4 in the Appendix. Thus, the analytic tractability as described above provides further motivation behind the specifications of the spatial-temporal processes for practical purposes, since, an efficient way for evaluating the predictive density at an out-of-sample point is particularly crucial in order to effectuate our stacking algorithm.

4.4. Stacking algorithm. We collect samples from $p(\beta, z \mid \chi, M)$, where $\chi = \{y, X, \tilde{X}, \mathcal{L}\}$ denotes the data and M specifies other parameters that must be conditioned for accessible posterior sampling. Following Yao et al. (2018), we devise a stacking algorithm for (7) based on predictive densities. Given a collection of candidate models $\mathcal{M} = \{M_1, \dots, M_G\}$, we find the probability distribution in $\mathcal{C} = \left\{ \sum_{g=1}^G w_g p(\cdot \mid \chi, M_g) : \sum_{g=1}^G w_g = 1, w_g \geq 0 \right\}$ by solving for the optimal stacking weights $w = (w_1, \dots, w_G)$ as the solution to the optimisation problem

$$\max_{w_1, \dots, w_G} \frac{1}{n} \sum_{i=1}^n \log \sum_{g=1}^G w_g p(y(\ell_i) \mid \chi_{-i}, M_g), \quad w_g \geq 0, \sum_{g=1}^G w_g = 1, \quad (18)$$

where $\chi_{-i} = (y_{-i}, X_{-i}, \tilde{X}_{-i}, \mathcal{L}_{-i})$, i.e., the data excluding the i th observation.

Solving for w in (18) involves the leave-one-out predictive density $p(y(\ell_i) \mid \chi_{-i}, M_g)$ for each i and g . For each g , we require n evaluations of the leave-one-out predictive densities to sample from (9) under M_g , given data χ_{-i} for $i = 1, \dots, n$. Following Vehtari et al. (2017), we apply K -fold cross-validation for faster evaluation of these densities. We randomly permute the data and construct K blocks using consecutive indices. Let $\chi_{[k]} = (y_{[k]}, X_{[k]}, \tilde{X}_{[k]}, \mathcal{L}_{[k]})$ be the k th block of size n_k and $\chi_{[-k]} = \{y_{[-k]}, X_{[-k]}, \tilde{X}_{[-k]}, \mathcal{L}_{[-k]}\}$ be its complement of size $(n - n_k)$ for $k = 1, \dots, K$. For each k , we fit M_g to $\chi_{[-k]}$ as we draw S samples $\{\beta_{k,l}^{(s)}, z_{k,l}^{(s)}\}_{s=1}^S \sim p((\gamma^T, q^T)^T \mid \chi_{[-k]}, M_g)$ as given in (9).

Estimating M_g on $\chi_{[-k]}$ requires a substantial computation dominated by Cholesky decompositions of matrices of size $\sim O(n)$ under both independent and multivariate process specifications. Under the independent process specification, instead of computing the Cholesky factor of $R_j(\mathcal{L}_{[-k]})$ for every $\chi_{[-k]}$, which would cost $O(Kn^3)$ flops, we execute an efficient block Givens rotation (Golub and Van Loan, 2013, Section 5.1.8) for faster evaluation of Cholesky factors of the K submatrices of $R_j(\mathcal{L})$ taking $O(Kn^3/4)$ operations for all blocks (see Algorithm A1 in the Appendix). Our algorithm is a block-level variant of Kim et al. (2002). For each $z_{k,l}^{(s)} = (z_{1,k,l}^{(s)\top}, \dots, z_{r,k,l}^{(s)\top})^\top$ where $z_{k,l}^{(s)}$ is $(n - n_k)r \times 1$, we draw posterior samples of $\tilde{z}_{k,l}^{(s)} = (\tilde{z}_{1,k,l}^{(s)\top}, \dots, \tilde{z}_{r,k,l}^{(s)\top})^\top$, the spatially-temporally varying $n_k r \times 1$ regression coefficients at the n_k left-out locations, $\mathcal{L}_{[k]}$ using (16) (see Section 4.3), which we use to evaluate $p(y(\ell_i) \mid \chi_{-i}, M_g)$. If $y(\ell_i) \in \chi_{[k]}$, then

$$p(y(\ell_i) \mid \chi_{-i}, M_g) \approx \frac{1}{S} \sum_{s=1}^S \text{EF} \left(y(\ell_i) \mid x(\ell_i)^\top \beta_{k,l}^{(s)} + \tilde{x}(\ell_i)^\top \tilde{z}_{k,l}^{(s)}(\ell_i); b_i, \psi_y \right), \quad (19)$$

where $r \times 1$ vector $\tilde{z}_{k,l}^{(s)}(\ell_i) = (\tilde{z}_{1,k,l}^{(s)}(\ell_i), \dots, \tilde{z}_{r,k,l}^{(s)}(\ell_i))^\top$ and $\text{EF}(y_0 \mid \eta_0; b, \psi)$ is the density of $\text{EF}(\eta_0; b, \psi)$ as defined in Section 2.1 evaluated at $y_0 \in \mathcal{Y}$. We repeat these steps for each of the G models and use (19) to solve the optimisation problem (18) using convex programming routines. Posterior inference for quantities of interest subsequently proceeds from the “stacked posterior”,

$$\tilde{p}(\cdot \mid \chi) = \sum_{g=1}^G \hat{w}_g p(\cdot \mid \chi, M_g), \quad (20)$$

where \hat{w}_g are optimal weights from (18); see Algorithm A2 in the Appendix.

Unlike MCMC, this stacking algorithm easily distributes independent tasks across multiple computing nodes and accrues substantial computational gains. The predictive stacking algorithm expends $O(G^\alpha + c^{-1}GKr n^3/4)$ flops for some $\alpha > 0$, where r , G and K are as defined earlier and c is the number of processing cores available in parallel. We use the package CVXR (Fu et al., 2020) in the R statistical computing environment by applying disciplined convex programming (2005 Stanford University Department of Electrical Engineering PhD thesis by M. Grant), while also confirming the convexity of the problem, and find the stacking weights in polynomial time $O(G^\alpha)$ using an interior-point algorithm. We use Mosek (ApS, 2023) and ECOSolveR (Fu and Narasimhan, 2023) to calculate stacking weights.

5. SIMULATION

5.1. Simulated data. We evaluate predictive performance of our proposed methods using two simulated datasets each of sample size n , with space-time coordinates sampled uniformly inside $[0, 1]^2 \times [0, 1]$, one with each varying coefficients are modelled as an independent spatial-temporal process, and the other assumes the varying coefficients are jointly a multivariate spatial-temporal process. We simulate the responses as Poisson count data $y(\ell) \sim \text{Poisson}(\exp(\eta(\ell)))$, where $\eta(\ell) = x(\ell)^T \beta + \tilde{x}(\ell)^T z(\ell)$. In each case, $x(\ell)$ is 2×1 consisting of an intercept and one predictor sampled from the standard normal distribution, and, the fixed effects $\beta = (5, -0.5)$. We set $\tilde{x}(\ell) = x(\ell)$, deeming all covariates to have spatially-temporally varying coefficients. Under the independent process assumption, $z_j(\ell) \sim \mathcal{GP}(0, \sigma_{z_j}^2 R_j(\cdot, \cdot))$ for $j = 1, 2$ with $\sigma_{z_1}^2 = 0.25$, $\sigma_{z_2}^2 = 0.5$ and, $(\phi_{11}, \phi_{21}) = (0.5, 2)$ and, $(\phi_{12}, \phi_{22}) = (1, 4)$. For the multivariate case, we assume $\Sigma = [(2, 0.5)^T, (0.5, 2)^T]^T$ and $\phi_1 = 1$ and $\phi_2 = 2$. The choice of β in each simulated data is such that the generated data do not contain excessive zeros. The simulation experiments are conducted with n varying from 200 to 600 with a randomly chosen holdout sample of size $n_h = 100$ over a set of coordinates \mathcal{L}_h .

5.2. Posterior inference. We fit multivariate and independent process models to our data. In each case, we stack on the parameters $\{\theta_{\text{sp}}, \alpha_\epsilon\}$, where θ_{sp} denotes the collection of process parameters corresponding to spatial-temporal process model and α_ϵ is the boundary adjustment parameter. For the prior on β , we consider $\mu_\beta = 0$ and, $V_\beta = I_2$. For subsequent inference, we fix hyperparameters $\nu_\beta = 2.1$ and $\nu_z = \nu_{z_1} = \nu_{z_2} = 2.1$. This ensures finite second moment of the corresponding marginal prior distributions of β and z . The parameters α_ϵ and κ_ϵ in (7) specify the shape and scale parameters (α^* and κ^*) of the posterior distribution (9). If the data is on the boundary of the parameter space with a high frequency (e.g., Poisson data with excessive zeros), then inference can be sensitive to these parameters (Bradley and Clinch, 2024).

We formally handle the value of these parameters by stacking on several models with different choices of α_ϵ (since κ_ϵ is uniquely determined by α_ϵ for Poisson/binomial count and binary data). In each case, we fix the grid of boundary adjustment parameter as $G_{\alpha_\epsilon} = \{0.5, 0.75\}$. Finally, for fitting the multivariate, we choose candidate values of the spatial-temporal decay parameters so that the corresponding effective range is approximately between 20% and 80% of the maximum spatial and temporal inter-coordinate distances (see Banerjee et al., 2025, Chapter 2), $G_{\phi_1} = \{0.3, 0.7, 1.2\}$ and $G_{\phi_2} = \{0.5, 0.75, 1.5\}$. In this case, we consider a Cartesian product of the grids, which yields $2 \times 3 \times 3 = 36$ candidate tuples of $\{\theta_{\text{sp}}, \alpha_\epsilon\}$, and, hence, we stack on 36 models. For the simulated data with independent process specification, we instead sample 36 points $\{(\phi_{11}, \dots, \phi_{1r}), (\phi_{21}, \dots, \phi_{2r}), \alpha_\epsilon\}$ uniformly from $[0.3, 1.3]^r \times [0.4, 1.5]^r \times G_{\alpha_\epsilon}$. We use $K = 10$ for K -fold cross validation (Vehtari and Lampinen, 2002).

We also estimate a fully Bayesian model with prior distributions on the spatial process parameters using MCMC for comparison with predictive stacking. In addition to the same priors for the model parameters, as mentioned above, we assign uniform priors $U(0.1, 5)$ on all process parameters in θ_{sp} . Here, it is worth remarking that sampling from the joint posterior distribution,

for example using random walk Metropolis steps, suffers considerably from mixing and convergence issues because of the high-dimensional parameter space and weak identifiability of process parameters. This issue is only partially mitigated using adaptive Metropolis steps (Roberts and Rosenthal, 2009). The Gibbs sampling algorithm involves sampling from the conditional posterior distributions $p(\theta_{\text{sp}} \mid \beta, z, \xi, y)$ and $p(\beta, z, \xi, \mid \theta_{\text{sp}}, y)$, where the former involves an adaptive Metropolis update using the R package `spBayes` (Finley et al., 2015) and, the latter proceeds by sampling from (9) using the projections described in Section 4.2. Furthermore, we compare predictive stacking with the integrated nested Laplace approximation (INLA; Rue et al., 2009), a widely used method for approximate Bayesian inference. We implement our model in INLA under the conventional assumption that the discrepancy parameter μ equals zero. The computation is carried out within the R package `INLAspacetime` (Krainski et al., 2025), which uses the `cgeneric` interface from the R-INLA (Lindgren and Rue, 2015) software. We compare the predictive performance of our stacking algorithm with MCMC by computing the mean log point-wise predictive density (MLPD) for the locations held-out, given by $\text{MLPD}_{\text{stacking}} = n_h^{-1} \sum_{\ell \in \mathcal{L}_h} \log \sum_{g=1}^G \hat{w}_g p(y(\ell) \mid y, M_g)$, and $\text{MLPD}_{\text{MCMC}} = n_h^{-1} \sum_{\ell \in \mathcal{L}_h} \log p(y(\ell) \mid y)$. For INLA, we obtain an approximate MLPD $\hat{p}(y(\ell) \mid y)$ using samples from the approximated posterior distribution.

5.3. Results.

5.3.1. *Posterior learning and predictive performance.* Figures 1(a) and (b) show results for the multivariate process model fitted to the simulated Poisson count data. Figure 1(a) presents the overlaid posterior densities of the fixed effects obtained from the stacked posterior (blue) and MCMC (red), revealing practically indistinguishable posterior distributions. Figure 1(b) also displays a high agreement between predictive stacking and MCMC with respect to the posterior medians of the spatial-temporal random effects associated with the intercept (z_1) and slope z_2 . We note similar observations for the independent process model. We also notice that the posterior samples of the spatial-temporal process parameters do not necessarily concentrate around their true values, hence, demonstrating their weak identifiability. We observe similar patterns in the posterior distributions of the temporal (ϕ_{11} and ϕ_{12}) and spatial decay parameters (ϕ_{21} and ϕ_{22}) for the independent process model (Figure A1 in the Appendix).

Treating the fully Bayesian model with priors on θ_{sp} , which is fitted using MCMC, we find that the predictive performance of our proposed stacking algorithm becomes closer to MCMC as the sample size increases (Table 1). For example, in the case of the multivariate model fitted on simulated data with multivariate process, we see that the difference in mean log-pointwise predictive density of 100 held-out samples between MCMC and our proposed stacking algorithm drops from 6.1% at sample size 100 to 1.5% at sample size 500. Table 1 reveals that the predictive precision of the multivariate model is better than the independent process model even when the data are simulated from the latter. This is possibly due to – (i) the weak identifiability of the process parameters in the independent model, which has $2r$ process parameters compared to just 2 in the multivariate model, and (ii) the random selection of candidate values for the $2r$ process parameters in the independent model against Cartesian product over a grid of candidate values of 2 process parameters in the multivariate model. In summary, the independent process model

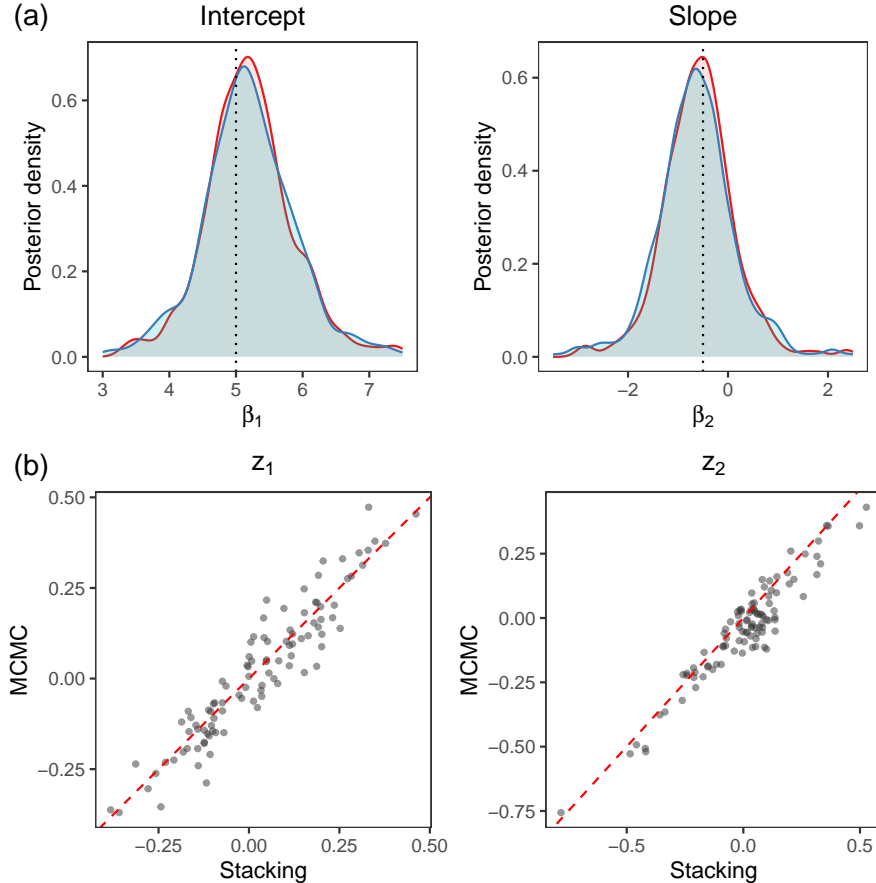


FIGURE 1. The multivariate spatial-temporal process model fitted on simulated Poisson count data: (a) posterior distributions of the intercept as well as the slope obtained from stacking (blue) and MCMC (red) overlaid dotted vertical line showing their true values; (b) posterior medians of spatial-temporal random effects obtained by stacking and MCMC with the $y = x$ reference as a red dashed line.

does not necessarily deliver superior predictive inference compared to the multivariate model in the presence of weakly identified parameters. We observe similar trends in the simulated binomial count and binary data (see Tables A1 and A2 in the Appendix).

Moreover, we compare predictive stacking and INLA for a spatially-temporally varying coefficient Poisson regression model by evaluating predictive performance using MLPD and examining computational runtimes, highlighting the trade-off between accuracy and efficiency. We summarize our findings in Table 2. In our INLA experiments, s_{grid} denotes the maximum edge length in the two-dimensional spatial mesh (see Figure A4 in the Appendix), and t_{grid} denotes the length between equispaced temporal grid points. We observe that predictive stacking consistently offers superior predictive performance compared to INLA, even when the latter is fitted with finer mesh resolutions. Although finer meshes provide a more detailed discretization of the spatial-temporal domain, predictive performance does not necessarily improve with increased resolution. This behaviour is largely an artefact of analysing irregularly spaced data within the INLA framework, as

Data generative process model	Model	Method	Sample size (n)				
			$n = 100$	$n = 200$	$n = 300$	$n = 400$	$n = 500$
Multivariate	Multivariate	Stacking	-3.67	-3.62	-3.55	-3.45	-3.39
		MCMC	-3.46	-3.44	-3.37	-3.36	-3.34
	Independent	Stacking	-3.81	-3.75	-3.68	-3.57	-3.49
		MCMC	-3.58	-3.49	-3.41	-3.32	-3.27
Independent	Multivariate	Stacking	-3.65	-3.59	-3.49	-3.41	-3.29
		MCMC	-3.58	-3.51	-3.42	-3.30	-3.20
	Independent	Stacking	-3.79	-3.76	-3.72	-3.52	-3.38
		MCMC	-3.53	-3.46	-3.34	-3.22	-3.14

TABLE 1. Predictive performance of stacking and MCMC under correct and misspecified spatial-temporal models on simulated Poisson counts. All values correspond to mean log-pointwise predictive density (MLPD) at 100 held-out locations, based on 5 replications.

	Sample size	Predictive stacking	INLA ($s_{\text{grid}}, t_{\text{grid}}$)		
			(0.5, 0.2)	(0.25, 0.1)	(0.15, 0.1)
MLPD	100	-3.61	-3.87	-3.94	-3.96
	200	-3.53	-3.82	-3.89	-3.85
	300	-3.51	-3.78	-3.79	-3.64
	400	-3.46	-3.75	-3.65	-3.45
Runtime	100	2.9	8.7	35.5	138.2
	200	9.9	8.8	35.5	139.1
	300	31.8	8.8	36.6	149.6
	400	61.5	8.9	36.9	153.2

TABLE 2. Comparison of predictive performance and execution times between predictive stacking and INLA under different mesh resolutions on spatial-temporal point-referenced Poisson count data with varying sample sizes.

finer meshes introduce additional nodes in regions without observations. In these areas, the latent field is poorly constrained, and INLA relies more heavily on the smoothness assumption rather than the data, which can inflate uncertainty and may degrade predictive performance. Moreover, INLA’s reliance on Laplace approximation to handle high-dimensional latent processes can limit the flexibility of the inference, especially in models with multiple spatial-temporal processes, such as our spatially-temporally varying coefficient model. Here, it is also important to recognize that our predictive stacking approach and INLA differ fundamentally, since the former aggregates predictive

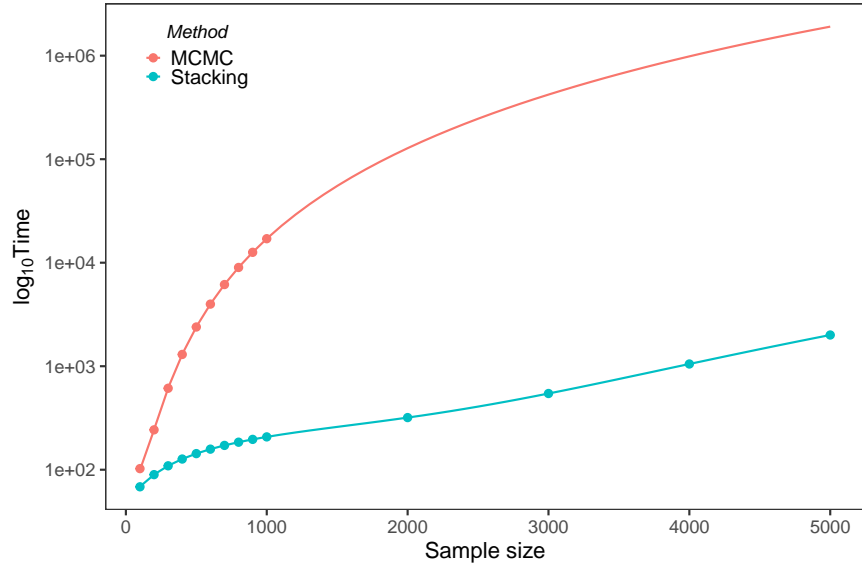


FIGURE 2. Comparison of runtimes of our proposed stacking algorithm and MCMC under the multivariate process assumption. Stacking demonstrates significantly faster execution times across various sample sizes compared to the MCMC algorithms.

distributions across candidate models, whereas the latter delivers inference by approximating the posterior distribution.

5.3.2. *Runtime comparison.* Figure 2 reveals that predictive stacking is, on average, about 500 times faster than MCMC further corroborating the efficiency of predictive stacking as an alternative to MCMC. We have implemented our predictive stacking algorithm within the R statistical computing environment (<https://www.r-project.org/>), where the code was written in C++ and Fortran leveraging BLAS and LAPACK libraries for efficient matrix operations. We execute the programs for runtime comparisons on hardware equipped with an 1-Intel(R) Xeon(R) Gold 6140 CPU @ 2.30GHz processor with 36 cores and 1 thread per core, totalling 36 possible threads for parallel computing. The runtime for predictive stacking reported here is based on execution using 6 cores only, in order to reflect realistic computational resources in contemporary personal computers. We compare the runtime of our proposed algorithm with the adaptive Metropolis-within-Gibbs algorithm that implements full Bayesian inference. Earlier benchmarks for MCMC-based inference for spatial GLMs, such as those reported by *spBayes*, indicate that computational demands become impractical when the sample size $n \sim 10^3$, or higher. In comparison, our proposed method achieves reasonable execution times for datasets with $n \sim 10^4$.

6. NORTH AMERICAN BREEDING BIRD SURVEY

Terrestrial birds were sampled annually on routes (approximately 40.23 km with point counts every 0.8 km) throughout the United States and Canada as part of the North American Breeding Bird

Survey (Ziolkowski Jr. et al., 2022). We analyse the number of migrant birds observed at different locations across the United States with the goal of predicting their numbers at an arbitrary location.

Our key inferential objective is to evaluate how the impact of nearby vehicles and external noise varies over space and time. We used 2,396 spatial coordinates between 2010 and 2019 at which the number of migrant birds were recorded. We aggregated the count data of different species within each spatial unit, since very few locations recorded counts for more than one species. We consider two explanatory variables, “car” and “noise”. The former represents tallies of vehicles passing survey points during each 3-minute count, and the latter reports unrelated excessive noise at each point from sources other than passing vehicles (for example, from construction work). The presence of excessive noise is defined as noise lasting more than 45 seconds that significantly interferes with the observer’s ability to hear birds at the location during the sampling period. These are mapped to the same GPS coordinates in the form of latitude and longitude that reference the avian counts.

The existing analysis has focused on modelling species-level variability and does not account for spatial-temporal correlation. For example, Link and Sauer (1997) and Sauer and Link (2011) study the route-level population trajectories of a species and observer effects using quasi-likelihood approaches and a Bayesian hierarchical log-linear model, respectively. Sauer and Link (2011) elaborates on the practical difficulties arising from convergence issues that require a limited number of MCMC iterations for moderately large datasets. Furthermore, their model featured random effects of a much lower dimension than we have in our proposed model (7). In addition, none of the previous analyses uses spatial random effects in order to model spatial variability in their log-linear model, whereas we utilise available geographic coordinates of the routes to build spatial-temporal processes to account for dependencies in the avian point count data within a rich modelling framework. This framework enables us to account for large scale variation in the mean using explanatory variables (for example the presence of excessive noise from vehicles) so the latent process evinces the residual spatial-temporal association in bird counts that can indicate lurking factors affecting the avian population.

We apply a spatial-temporal Poisson regression model in (7) with the multivariate spatial-temporal process to analyse the counts of migrant birds. The predictors ‘car’ and ‘noise’ have spatially-temporally varying regression coefficients with the correlation function in (12). We assumed $\Psi = 1.5I_3 + 0.51_31_3^T$. We implement the proposed stacking with $G_{\phi_2} = \{40, 800, 1000\}$ (the effective spatial range is approximately 20%, 50% and 70% of the maximum distance between sites), $G_{\phi_1} = \{0.5, 1, 2\}$ and $G_{\alpha_\epsilon} = \{0.5, 0.75\}$. We also fit a non-spatial-temporal Poisson regression model and a spatial-temporal model with the intercept as the only predictor with varying coefficients, with the latter using our predictive stacking framework. Table 3 presents posterior summaries of β (the global regression coefficients that does not vary over space and time) for the intercept, ‘car’ and ‘noise’. The global intercept is significantly larger than zero, which contributes approximately 2.4 units to the count with 95% credible interval (2.1, 2.8) in the presence of no passing cars or excessive noise. Neither the number of cars nor levels of excessive noise seem to significantly impact the count in terms of global effects. The last row of Table 3 presents the estimated bird count averaged over all observed spatial-temporal coordinates in the data set. This is obtained from the posterior predictive distribution of the average bird count and provides us

Model parameters	Model		
	Non-spatial-temporal	Intercept-only spatial-temporal	Spatially-temporally varying coefficients
Intercept	2.182 (2.165, 2.195)	0.946 (0.832, 1.063)	0.874 (0.729, 1.109)
Car	0.0003 (0.0002, 0.0004)	0.0002 (-0.0004, 0.0008)	0.003 (-0.021, 0.029)
Noise	0.026 (0.023, 0.028)	0.0121 (-0.007, 0.032)	0.007 (-0.104, 0.118)
Average bird count	9.749 (9.572, 9.819)	5.136 (4.099, 10.984)	9.472 (9.455, 10.218)

TABLE 3. North American Breeding Bird Survey (2010-19): Posterior summary of global regression coefficients and average bird count over all spatial-temporal coordinates. Values in parenthesis represent 2.5% and 97.5% quantiles.

with an estimate of the relative influence of the spatially-temporally varying component over the global effects. Here, we see that the spatially-temporally varying coefficients increase the estimate of counts (≈ 9.7) by a factor of 4 over the estimated bird count of ≈ 2.4 estimated from the global effects. This estimate of the average bird count is consistent with what one would obtain from customary GLMs with fixed effects only, but simple GLMs will not offer insights into the spatially and temporally varying impact of predictors. Also, the intercept-only spatial-temporal model is underestimating the response, which may be due to excessive smoothing, where the random effects are not capturing local variations properly. This suggests the importance of accounting for spatial-temporal variations in regression slopes to accurately model the response.

Figures 3(a) and (b) reveal the space-time varying impact of the predictors ‘car’ and ‘noise’. In Fig. 3(a) we see significant positive impact (red) of ‘car’ in the Niland and Palo Verde regions of Imperial county, California, (in the south-west corner) rather consistently between 2010 and 2012. These elevated spatial-temporal coefficients and higher numbers of cars in these regions (not shown) produce higher than average estimates of bird counts there. We observe a similar pattern in parts of North Dakota and South Dakota between 2015 and 2019. Figure 3(b) reveals a positive impact (red) of ‘noise’ in the spatial-temporal random effects in northern Minnesota from 2011 to 2015. While this area experiences persistently low levels of ‘noise’ (not shown), the high values of the coefficients produce higher estimates of bird counts. These spatially-temporally varying coefficients capture the local impact of predictors to adjust the global effects from Table 3. Appendix D presents additional data analysis. Lastly, while predictive stacking delivered inference in 20 minutes using 6 cores, an adaptive Metropolis-within-Gibbs algorithm anticipates at least 30,000 iterations for convergence with each iteration taking 20 seconds on average. Hence, stacking offers speed-ups of over 500 times over MCMC.

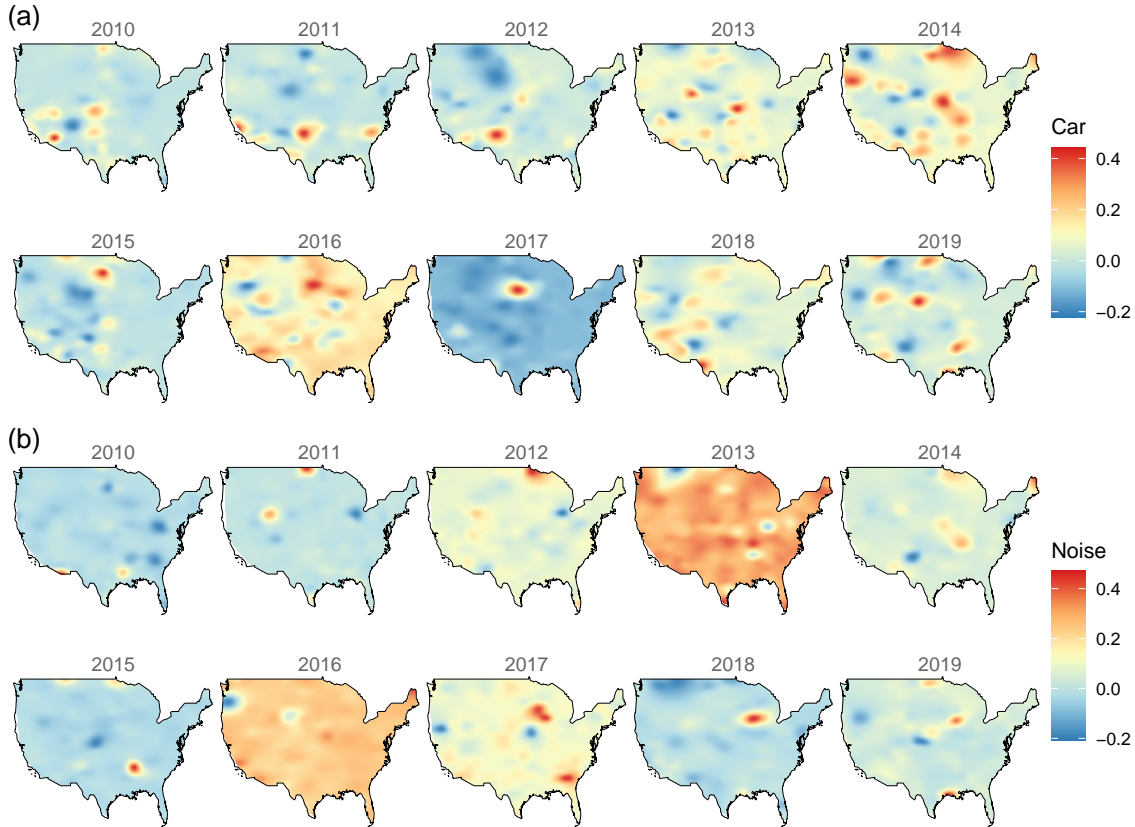


FIGURE 3. North American Breeding Bird Survey (2010-19): Interpolated surfaces of posterior median of spatial-temporal random effects in the slope of the variables (a) ‘car’ and, (b) ‘noise’ obtained by our proposed stacking algorithm.

7. DISCUSSION

We developed Bayesian predictive stacking as an effective tool to estimate spatially-temporally varying regression coefficients and carry out predictive inference on non-Gaussian spatial-temporal data. Our method effectively combines inference across different closed-form posterior distributions by circumventing inference on weakly identified parameters. Rather than a replacement or competitor to MCMC, which, in principle, offers full uncertainty quantification of weakly identified parameters, we see stacking as an extremely viable tool in the spatial analysts’ armour when primary inference concerns the process itself, regression coefficients, variance components and predictions. Our proposed stacking framework can be explored further in at least two directions of active research in scalable spatial analysis. First, we note that the current article has dealt with full Gaussian process models, which involves the Cholesky factorization of a dense covariance matrix incurring a computational cost of $\sim O(n^3)$ flops. This can be significantly mitigated by replacing the full Gaussian process with processes that can scale inference to massive amounts of data (see. e.g., [Datta et al., 2016](#); [Banerjee, 2017](#); [Heaton et al., 2019](#); [Peruzzi et al., 2022](#), and references therein for a burgeoning literature on scalable Gaussian processes). Here, we do not anticipate substantial modifications since scalable processes retain similar parametric forms and conjugacy of conditional

posteriors (see, e.g., [Datta et al., 2016](#); [Zhang et al., 2019](#); [Banerjee, 2020](#)) and stacking can be executed over a grid of their covariance kernel parameters as described here. A different avenue for scalable stacking is federated Bayesian learning and transfer learning, where inference is carried out on distributed data subsets (see, e.g., [Guhaniyogi and Banerjee, 2018](#); [Vehtari et al., 2020](#); [Guhaniyogi et al., 2023](#)) and the resulting subset posteriors are combined via stacking ([Presicce and Banerjee, 2025](#)) providing a complementary route to computational scalability.

A second direction of research under exploration attempts to address what we acknowledge is a limitation of the current methodology. Note that predictive stacking relies on a discrete grid over a subset of model parameters. If the number of such parameters (typically hyperparameters in covariance kernels) in the model is very large, then computation becomes impractical because the number of candidate models grows exponentially with the dimension of the grid. For most spatial and spatial-temporal models, this issue seldom arises in practice, as the number of weakly identified parameters requiring conditioning is typically small. However in other settings (e.g., highly multivariate responses [Zhang et al., 2021](#); [Zhang and Banerjee, 2022](#); [Dey et al., 2022](#); [Perruzzi et al., 2025](#)), where we seek to jointly model multiple spatial processes, hyperparameters in the resulting spatial cross-covariance functions can become high-dimensional and our current method becomes computationally infeasible. While some mitigation of this problem is achieved by using a random sample of values of these parameters (rather than every lattice point on the high-dimensional grid), there is ample scope for research in this domain. One promising direction is the development of methodologies that reduce the effective number of candidate models through principled compression of the parameter space, while preserving the inferential objectives of stacking. Such approaches may offer a pathway to both computational scalability and improved flexibility in high-dimensional settings. Finally, it remains an open problem to investigate the effectiveness of predictive stacking for non-stationary processes with spatially-varying covariance kernels ([Paciorek and Schervish, 2006](#)). In these models covariance kernel parameters are themselves modelled as spatial processes, so conditioning on their realisations is impractical. However, recent developments in [Coube-Sisqueille et al. \(2025\)](#), which use scalable processes to model covariance kernel parameters to achieve dimension reduction, can offer promising avenues of research to adapt such models to be analysed using predictive stacking.

ACKNOWLEDGEMENT

This work used computational and storage services associated with the Hoffman2 Shared Cluster provided by UCLA Office of Advanced Research Computing’s Research Technology Group. Sudipto Banerjee and Soumyakanti Pan were supported by two research grants from the National Institute of Environmental Health Sciences (NIEHS), one grant from the National Institute of General Medical Science (NIGMS) and another from the Division of Mathematical Sciences of the National Science Foundation (NSF-DMS). Lu Zhang was supported by NIEHS (P30ES007048, P20HL176204, R01ES031590). J. R. Bradley was supported by NSF-DMS.

DATA AND CODE AVAILABILITY

All code and data required to reproduce the results and findings in this article are openly available at <https://github.com/SPan-18/stvcGLMstack>. The code is disseminated via the development version of the R package `spStack` (Pan and Banerjee, 2024), available for download from the GitHub repository <https://github.com/SPan-18/spStack-dev>. The North American Breeding Bird survey database is openly available at <https://doi.org/10.5066/P97WAZE5>.

REFERENCES

- Milton Abramowitz and Irene A. Stegun, editors. *Handbook of Mathematical Functions with Formulas, Graphs and Mathematical Tables*. Dover Publications, Inc., New York, 1965.
- MOSEK ApS. *MOSEK Rmosek package 9.3.22*, 2023. URL <https://docs.mosek.com/9.3/rmosek/index.html>.
- Sudipto Banerjee. High-Dimensional Bayesian Geostatistics. *Bayesian Analysis*, 12(2):583 – 614, 2017. doi: 10.1214/17-BA1056R. URL <https://doi.org/10.1214/17-BA1056R>.
- Sudipto Banerjee. Modeling massive spatial datasets using a conjugate Bayesian linear modeling framework. *Spatial Statistics*, 37:100417, 2020. ISSN 2211-6753. doi: 10.1016/j.spasta.2020.100417. URL <https://doi.org/10.1016/j.spasta.2020.100417>. Frontiers in Spatial and Spatio-temporal Research.
- Sudipto Banerjee, Alan E. Gelfand, and Brad P. Carlin. *Hierarchical Modeling and Analysis for Spatial Data*. Chapman and Hall/CRC, 3rd edition, 2025. doi: 10.1201/9781003401728. URL <https://doi.org/10.1201/9781003401728>.
- Jonathan R. Bradley and Madelyn Clinch. Generating independent replicates directly from the posterior distribution for a class of spatial hierarchical models. *Journal of Computational and Graphical Statistics*, 0(ja):1–32, 2024. doi: 10.1080/10618600.2024.2365728. URL <https://doi.org/10.1080/10618600.2024.2365728>.
- Jonathan R. Bradley, Scott H. Holan, and Christopher K. Wikle. Bayesian hierarchical models with conjugate full-conditional distributions for dependent data from the natural exponential family. *Journal of the American Statistical Association*, 115(532):2037–2052, 2020. doi: 10.1080/01621459.2019.1677471. URL <https://doi.org/10.1080/01621459.2019.1677471>.
- Leo Breiman. Stacked regressions. *Machine learning*, 24(1):49–64, 1996.
- Merlise Clyde and Edwin S Iversen. Bayesian model averaging in the m-open framework. *Bayesian theory and applications*, 14(4):483–498, 2013. doi: 10.1093/acprof:oso/9780199695607.003.0024. URL <https://doi.org/10.1093/acprof:oso/9780199695607.003.0024>.
- Sébastien Coube-Sisqueille, Sudipto Banerjee, and Benoît Liqueur. Nonstationary spatial process models with spatially varying covariance kernels. *Journal of Computational and Graphical Statistics*, (in press), 2025. doi: 10.1080/10618600.2025.2516020. URL <https://doi.org/10.1080/10618600.2025.2516020>.
- Abhirup Datta, Sudipto Banerjee, Andrew O. Finley, and Alan E. Gelfand. Hierarchical Nearest-Neighbor Gaussian Process Models for Large Geostatistical Datasets. *Journal of the American Statistical Association*, 111(514):800–812, 2016. doi: 10.1080/01621459.2015.1044091. URL

- <https://doi.org/10.1080/01621459.2015.1044091>.
- Victor De Oliveira. Bayesian prediction of clipped gaussian random fields. *Computational Statistics & Data Analysis*, 34(3):299–314, 2000. doi: 10.1016/S0167-9473(99)00103-6. URL [https://doi.org/10.1016/S0167-9473\(99\)00103-6](https://doi.org/10.1016/S0167-9473(99)00103-6).
- Victor De Oliveira, Benjamin Kedem, and David A. Short. Bayesian prediction of transformed gaussian random fields. *Journal of the American Statistical Association*, 92(440):1422–1433, 1997. doi: 10.1080/01621459.1997.10473663. URL <https://doi.org/10.1080/01621459.1997.10473663>.
- Debangana Dey, Abhirup Datta, and Sudipto Banerjee. Graphical gaussian process models for highly multivariate spatial data. *Biometrika*, 109(4):993–1014, 12 2022. ISSN 1464-3510. doi: 10.1093/biomet/asab061.
- Persi Diaconis and Donald Ylvisaker. Conjugate Priors for Exponential Families. *The Annals of Statistics*, 7(2):269 – 281, 1979. doi: 10.1214/aos/1176344611. URL <https://doi.org/10.1214/aos/1176344611>.
- P. J. Diggle, J. A. Tawn, and R. A. Moyeed. Model-based geostatistics. *Journal of the Royal Statistical Society Series C: Applied Statistics*, 47(3):299–350, 01 1998. ISSN 0035-9254. doi: 10.1111/1467-9876.00113. URL <https://doi.org/10.1111/1467-9876.00113>.
- Peng Ding. On the conditional distribution of the multivariate t distribution. *The American Statistician*, 70(3):293–295, 2016. doi: 10.1080/00031305.2016.1164756. URL <https://doi.org/10.1080/00031305.2016.1164756>.
- Andrew O. Finley, Sudipto Banerjee, and Alan E. Gelfand. spbayes for large univariate and multivariate point-referenced spatio-temporal data models. *Journal of Statistical Software*, 63(13): 1–28, 2015. doi: 10.18637/jss.v063.i13. URL <https://doi.org/10.18637/jss.v063.i13>.
- Anqi Fu and Balasubramanian Narasimhan. *ECOSolveR: Embedded Conic Solver in R*, 2023. URL <https://bnaras.github.io/ECOSolveR/>. R package version 0.5.5.
- Anqi Fu, Balasubramanian Narasimhan, and Stephen Boyd. CVXR: An R package for disciplined convex optimization. *Journal of Statistical Software*, 94(14):1–34, 2020. doi: 10.18637/jss.v094.i14. URL <https://doi.org/10.18637/jss.v094.i14>.
- Alan E. Gelfand, Hyon-Jung Kim, C. F. Sirmans, and Sudipto Banerjee. Spatial modeling with spatially varying coefficient processes. *Journal of the American Statistical Association*, 98(462):387–396, 2003. doi: 10.1198/016214503000170. URL <https://doi.org/10.1198/016214503000170>.
- T. Gneiting and P. Guttorp. Continuous-parameter spatio-temporal processes. In A.E. Gelfand, P.J. Diggle, M. Fuentes, and P Guttorp, editors, *Handbook of Spatial Statistics*, Chapman & Hall CRC Handbooks of Modern Statistical Methods, pages 427–436. Taylor and Francis, 2010. doi: 10.1201/9781420072884. URL <https://doi.org/10.1201/9781420072884>.
- Gene H. Golub and Charles F. Van Loan. *Matrix Computations*. Johns Hopkins University Press, Philadelphia, PA, 4th edition, 2013. doi: 10.1137/1.9781421407944. URL <https://doi.org/10.1137/1.9781421407944>.
- Rajarshi Guhaniyogi and Sudipto Banerjee. Meta-kriging: Scalable bayesian modeling and inference for massive spatial datasets. *Technometrics*, 60(4):430–444, 2018. doi: 10.1080/00401706.2018.1437474. URL <https://doi.org/10.1080/00401706.2018.1437474>.

- Rajarshi Guhaniyogi, Cheng Li, Terrance Savitsky, and Sanvesh Srivastava. Distributed Bayesian Inference in Massive Spatial Data. *Statistical Science*, 38(2):262 – 284, 2023. doi: 10.1214/22-STS868. URL <https://doi.org/10.1214/22-STS868>.
- A. K. Gupta and D. K. Nagar. *Matrix Variate Distributions*. Chapman and Hall/CRC, New York, 1999. doi: 10.1201/9780203749289. URL <https://doi.org/10.1201/9780203749289>.
- M. Haran. Gaussian random field models for spatial data. In *Markov chain Monte Carlo Handbook Eds. Brooks, S.P., Gelman, A.E. Jones, G.L. and Meng, X.L.*, pages 449–478. Chapman and Hall/CRC, 2011.
- Patrick J Heagerty and Subhash R Lele. A composite likelihood approach to binary spatial data. *Journal of the American Statistical Association*, 93(443):1099–1111, 1998. doi: 10.1080/01621459.1998.10473771. URL <https://doi.org/10.1080/01621459.1998.10473771>.
- Matthew J. Heaton, Abhirup Datta, Andrew O. Finley, Reinhard Furrer, Joseph Guinness, Rajarshi Guhaniyogi, Florian Gerber, Robert B. Gramacy, Dorit Hammerling, Matthias Katzfuss, Finn Lindgren, Douglas W. Nychka, Furong Sun, and Andrew Zammit-Mangion. A case study competition among methods for analyzing large spatial data. *Journal of Agricultural, Biological, and Environmental Statistics*, 24(3):pp. 398–425, 2019. doi: 10.1007/s13253-018-00348-w. URL <https://doi.org/10.1007/s13253-018-00348-w>.
- Jennifer A. Hoeting, David Madigan, Adrian E. Raftery, and Chris T. Volinsky. Bayesian model averaging: a tutorial (with comments by M. Clyde, David Draper and E. I. George, and a rejoinder by the authors). *Statistical Science*, 14(4):382 – 417, 1999. doi: 10.1214/ss/1009212519. URL <https://doi.org/10.1214/ss/1009212519>.
- John Hughes and Murali Haran. Dimension reduction and alleviation of confounding for spatial generalized linear mixed models. *Journal of the Royal Statistical Society. Series B: Statistical Methodology*, 75(1):139–159, January 2013. doi: 10.1111/j.1467-9868.2012.01041.x. URL <https://doi.org/10.1111/j.1467-9868.2012.01041.x>.
- Tae Yoon Kim, Jeong Soo Park, and Dennis D Cox and. Fast algorithm for cross-validation of the best linear unbiased predictor. *Journal of Computational and Graphical Statistics*, 11(4): 823–835, 2002. doi: 10.1198/106186002826. URL <https://doi.org/10.1198/106186002826>.
- Elias Teixeira Krainski, Finn Lindgren, and Haavard Rue. *INLAspacetime: Spatial and Spatio-Temporal Models using 'INLA'*, 2025. URL <https://CRAN.R-project.org/package=INLAspacetime>. R package version 0.1.12.
- Tri Le and Bertrand Clarke. A Bayes interpretation of stacking for m-complete and m-open settings. *Bayesian Analysis*, 12(3):807–829, 2017. doi: 10.1214/16-BA1023. URL <https://doi.org/10.1214/16-BA1023>.
- Finn Lindgren and Håvard Rue. Bayesian spatial modelling with R-INLA. *Journal of Statistical Software*, 63(19):1–25, 2015. doi: 10.18637/jss.v063.i19. URL <https://doi.org/10.18637/jss.v063.i19>.
- William A. Link and John R. Sauer. Estimation of population trajectories from count data. *Biometrics*, 53(2):488–497, 1997. doi: 10.2307/2533952. URL <https://doi.org/10.2307/2533952>.
- David Madigan, Adrian E Raftery, C Volinsky, and Jennifer Hoeting. Bayesian model averaging. In *Proceedings of the AAAI Workshop on Integrating Multiple Learned Models, Portland, OR*,

- pages 77–83, 1996.
- K. V. Mardia and C. R. Goodall. Spatial-temporal analysis of multivariate environmental monitoring data. *Multivariate Environmental Statistics*, 1993.
- Charles E. McCulloch and Shayle R. Searle. *Generalized, linear, and mixed models*. Wiley Series in Probability and Statistics. John Wiley & Sons, 2001. doi: 10.1002/0471722073. URL <https://doi.org/10.1002/0471722073>.
- Christopher J. Paciorek and Mark J. Schervish. Spatial modelling using a new class of nonstationary covariance functions. *Environmetrics*, pages 483–506, 2006. doi: 10.1002/env.785. URL <https://doi.org/10.1002/env.785>.
- Soumyakanti Pan and Sudipto Banerjee. *spStack: Bayesian Geostatistics Using Predictive Stacking*, 2024. URL <https://CRAN.R-project.org/package=spStack>. R package version 1.1.2.
- Michele Peruzzi, Sudipto Banerjee, and Andrew O. Finley. Highly scalable Bayesian geostatistical modeling via meshed Gaussian processes on partitioned domains. *Journal of the American Statistical Association*, 117(538):969–982, 2022. doi: 10.1080/01621459.2020.1833889. URL <https://doi.org/10.1080/01621459.2020.1833889>.
- Michele Peruzzi, Sudipto Banerjee, David B. Dunson, and Andrew O. Finley. Gridding and Parameter Expansion for Scalable Latent Gaussian Models of Spatial Multivariate Data. *Bayesian Analysis*, pages 1 – 27, 2025. doi: 10.1214/25-BA1515. URL <https://doi.org/10.1214/25-BA1515>.
- Luca Presicce and Sudipto Banerjee. Bayesian transfer learning for artificially intelligent geospatial systems: A predictive stacking approach, 2025. URL <https://arxiv.org/abs/2410.09504>.
- Gareth O. Roberts and Jeffrey S. Rosenthal. Examples of adaptive MCMC. *Journal of Computational and Graphical Statistics*, 18(2):349–367, 2009. doi: 10.1198/jcgs.2009.06134. URL <https://doi.org/10.1198/jcgs.2009.06134>.
- Håvard Rue, Sara Martino, and Nicolas Chopin. Approximate Bayesian Inference for Latent Gaussian models by using Integrated Nested Laplace Approximations. *Journal of the Royal Statistical Society Series B: Statistical Methodology*, 71(2):319–392, 04 2009. ISSN 1369-7412. doi: 10.1111/j.1467-9868.2008.00700.x. URL <https://doi.org/10.1111/j.1467-9868.2008.00700.x>.
- Arkajyoti Saha, Abhirup Datta, and Sudipto Banerjee. Scalable predictions for spatial probit linear mixed models using nearest neighbor gaussian processes. *Journal of Data Science*, 20(4): 533–544, 2022. ISSN 1680-743X. doi: 10.6339/22-JDS1073. URL <https://doi.org/10.6339/22-JDS1073>.
- John R. Sauer and William A. Link. Analysis of the north american breeding bird survey using hierarchical models. *The Auk*, 128(1):87–98, 01 2011. ISSN 1938-4254. doi: 10.1525/auk.2010.09220. URL <https://doi.org/10.1525/auk.2010.09220>.
- Aki Vehtari and Jouko Lampinen. Bayesian Model Assessment and Comparison Using Cross-Validation Predictive Densities. *Neural Computation*, 14(10):2439–2468, 10 2002. ISSN 0899-7667. doi: 10.1162/08997660260293292. URL <https://doi.org/10.1162/08997660260293292>.
- Aki Vehtari, Andrew Gelman, and Jonah Gabry. Practical Bayesian model evaluation using leave-one-out cross-validation and waic. *Statistics and Computing*, 27(5):1413–1432, sep 2017. ISSN 0960-3174. doi: 10.1007/s11222-016-9696-4. URL <https://doi.org/10.1007/s11222-016-9696-4>.

- Aki Vehtari, Andrew Gelman, Tuomas Sivula, Pasi Jylänki, Dustin Tran, Swupnil Sahai, Paul Blomstedt, John P. Cunningham, Frank Schorfheide, and Yuling Yao. A framework for bayesian inference on partitioned data. *Journal of Machine Learning Research*, 21(87):1–49, 2020. URL <http://jmlr.org/papers/v21/18-817.html>.
- David H Wolpert. Stacked generalization. *Neural networks*, 5(2):241–259, 1992.
- Yuling Yao, Aki Vehtari, Daniel Simpson, and Andrew Gelman. Using stacking to average Bayesian predictive distributions (with discussion). *Bayesian Analysis*, 13(3):917–1007, 2018. doi: 10.1214/17-BA1091. URL <https://doi.org/10.1214/17-BA1091>.
- Yuling Yao, Gregor Pirš, Aki Vehtari, and Andrew Gelman. Bayesian hierarchical stacking: Some models are (somewhere) useful. *Bayesian Analysis*, 1(1):1–29, 2021. doi: 10.1214/21-BA1287. URL <https://doi.org/10.1214/21-BA1287>.
- Yuling Yao, Aki Vehtari, and Andrew Gelman. Stacking for Non-mixing Bayesian computations: The curse and blessing of multimodal posteriors. *Journal of Machine Learning Research*, 23(79):1–45, 2022. URL <http://jmlr.org/papers/v23/20-1426.html>.
- Lu Zhang and Sudipto Banerjee. Spatial factor modeling: A bayesian matrix-normal approach for misaligned data. *Biometrics*, 78(2):560–573, 2022. doi: 10.1111/biom.13452. URL <https://doi.org/10.1111/biom.13452>.
- Lu Zhang, Abhirup Datta, and Sudipto Banerjee. Practical bayesian modeling and inference for massive spatial data sets on modest computing environments†. *Statistical Analysis and Data Mining: The ASA Data Science Journal*, 12(3):197–209, 2019. doi: 10.1002/sam.11413. URL <https://doi.org/10.1002/sam.11413>.
- Lu Zhang, Sudipto Banerjee, and Andrew O. Finley. High-dimensional multivariate geostatistics: A Bayesian matrix-normal approach. *Environmetrics*, 32(4):e2675, 2021. doi: 10.1002/env.2675. URL <https://doi.org/10.1002/env.2675>.
- Lu Zhang, Wenpin Tang, and Sudipto Banerjee. Bayesian geostatistics using predictive stacking. *Journal of the American Statistical Association*, (In press), 2025. doi: 10.1080/01621459.2025.2566449. URL <https://doi.org/10.1080/01621459.2025.2566449>.
- Zhongwei Zhang, Reinaldo B. Arellano-Valle, Marc G. Genton, and Raphaël Huser. Tractable bayes of skew-elliptical link models for correlated binary data. *Biometrics*, 79(3):1788–1800, 08 2022. ISSN 0006-341X. doi: 10.1111/biom.13731. URL <https://doi.org/10.1111/biom.13731>.
- David Ziolkowski Jr., Michael Lutmerding, Veronica Aponte, and Marie-Anne Hudson. North American Breeding Bird Survey Dataset 1966 - 2021: U.S. Geological Survey data release, 2022. URL <https://doi.org/10.5066/P97WAZE5>.

APPENDIX A. DISTRIBUTION THEORY

A.1. Existence of improper prior on the discrepancy parameter. Reparametrization of the discrepancy parameter $\mu = (\mu_1, \dots, \mu_n)^\top$ into $q = -Q^\top D(\theta) \tilde{\mu}$, where $\tilde{\mu} = (\mu^\top, 0_n^\top, \mu_\beta^\top L_\beta^{-\top}, 0_{nr}^\top)^\top$ is essential for obtaining the GCM joint prior distribution on the model parameters, as outlined in (8). Our contribution here lies in proving two important results, Lemma A1 and Theorem A1,

that justifies constructing the improper prior that has not been addressed hitherto (Bradley and Clinch, 2024, Theorem 3.1). We assume familiarity with notations introduced in Section 3 of the main article. For convenience, rewrite H in the main article as $H = [(I_n : X_{n \times p} : \tilde{X}_{n \times nr})^\top; L_\gamma^{-1}]^\top$, where $L_\gamma = \text{blkdiag}(I_n, L_\beta, L_z)$.

Lemma A1. *If $H = [(I_n : X_{n \times p} : \tilde{X}_{n \times nr})^\top; L_\gamma^{-1}]^\top$ and $Q = [Q_1^\top : Q_2^\top]^\top$, where Q is $(2n + p + nr) \times n$ with Q_1 being $n \times n$, such that the n columns of Q are the unit norm orthogonal eigenvectors of P_H , the orthogonal projector on the column space of H , then $\text{rank}(Q_1) = n$.*

Proof. From our definitions, we note that $QQ^\top = I_{2n+p+nr} - P_H$, $P_H = H(H^\top H)^{-1}H^\top$, $Q^\top H = 0$ and $\text{rank}(Q) = n$. Define $H_1 = [I_n : X : \tilde{X}]$. It follows from $Q^\top H = 0$ that, $Q_1^\top H_1 + Q_2^\top L_\gamma^{-1} = 0$ and subsequently, $Q_2 = -L_\gamma^\top H_1^\top Q_1$, implying that $\mathcal{R}(Q_2) \subseteq \mathcal{R}(Q_1)$ where \mathcal{R} denotes row space of a matrix. Hence the rank of Q must equal $\dim(\mathcal{R}(Q_1))$, the number of independent rows of Q_1 . As $\text{rank}(Q) = n$, $\text{rank}(Q_1) = \dim(\mathcal{R}(Q_1)) = n$. \square

Theorem A1. *In the hierarchical model (7), assumption of a vague prior on the parameter μ leads to the improper prior on the parameter q , given by $p(q) \propto 1$.*

Proof. Recall that $q = -Q^\top D(\theta) \tilde{\mu}$ where $\tilde{\mu} = (\mu^\top, \mu_\gamma^\top L_\gamma^{-\top})^\top$ with $\mu_\gamma = (0_n^\top, \mu_\beta^\top, 0_{nr}^\top)^\top$, and $Q = [Q_1^\top : Q_2^\top]^\top$ is the $(2n + p + nr) \times n$ matrix as defined in Lemma A1, where Q_1 is $n \times n$ and Q_2 is $(n + p + nr) \times n$. Recall $D(\theta) = \text{blkdiag}(I_n, D_\gamma(\theta))$, where $D_\gamma(\theta) = \text{blkdiag}(\sigma_\xi^2 I_n, \sigma_\beta^2 I_p, D_z(\theta_z))$ with $\theta = \{\sigma_\xi^2, \sigma_\beta^2, \theta_z\}$. Then, we have $q = -Q_1^\top \mu - Q_2^\top D_\gamma(\theta) L_\gamma^{-1} \mu_\gamma$.

Consider the sequence of priors on the discrepancy parameter as $p_{1,k}(\mu) = \mathcal{N}(\mu \mid 0_n, \tau_k I_n)$ for a real sequence $\{\tau_k\}_{k \in \mathbb{N}}$ with $\tau_k > 0, \forall k \in \mathbb{N}$ such that $\lim_k \tau_k = +\infty$. By Lemma A1, for any k , the prior on q induced by $p_{1,k}$ has the density $p_{2,k}(q) = \mathcal{N}(q \mid -Q_2^\top D_\gamma(\theta) L_\gamma^{-1} \mu_\gamma, \tau_k Q_1^\top Q_1)$. Hence, the improper density $p_2(q) \propto 1$ arises from $\lim_k p_{2,k}(q) = p_2(q)$ for any $q \in \mathbb{R}^n$. \square

A.2. Derivation of posterior distribution. We derive the posterior distribution in (9) corresponding to the hierarchical model specified by (8) in the main article. The following result adapts the spatial intercept model of Theorem 3.1 in Bradley and Clinch (2024) to our spatially-temporally varying coefficient model, and, reformulates in a way that completely avoids the complicated conditional GCM distribution used previously in the literature Bradley and Clinch (2024), thus offering a comprehensive and simplified derivation of the posterior distribution (9),

Theorem A2. *Suppose $\{y_i : i = 1, \dots, n\}$ denotes responses distributed from the natural exponential family, x_i is $p \times 1$ predictor corresponding to the $p \times 1$ fixed effect β , \tilde{x}_i is the $r \times 1$ predictor with $r \times 1$ random slope $z_i = (z_{i1}, \dots, z_{ir})^\top$. Then, for the Bayesian hierarchical model*

$$\begin{aligned} y_i \mid \beta, z_i, \xi_i, \mu_i &\sim \text{EF}(x_i^\top \beta + \tilde{x}_i^\top z_i + \xi_i - \mu_i; b_i, \psi_y), \quad i = 1, \dots, n \\ (\gamma^\top, q^\top)^\top &\sim \text{GCM}(0_{2n+p+nr}, V, \alpha, \kappa, D, \pi; \psi), \end{aligned} \quad (\text{A1})$$

where $\gamma = (\xi^\top, \beta^\top, z^\top)^\top$, with fine-scale variation $\xi = (\xi_1, \dots, \xi_n)^\top$, $z = (z_1^\top, \dots, z_r^\top)^\top$, z_j is $n \times 1$ for each $j = 1, \dots, r$. The parameter $\theta = \{\sigma_\xi^2, \sigma_\beta^2, \theta_z\}$ denotes a collection of scale parameters with prior $\pi(\theta)$, and $(n + p + nr) \times (n + p + nr)$ matrix $D(\theta) = \text{blkdiag}(I_n, \sigma_\xi^2 I_n, \sigma_\beta^2 I_p, D_z(\theta_z))$ for $nr \times nr$ invertible matrix $D_z(\theta)$. The $(2n + p + nr) \times (2n + p + nr)$ matrix $V^{-1} = [H : Q]$ is

assumed known, where $(2n+p+nr) \times (n+p+nr)$ matrix $H = [(I, X, \tilde{X})^T, L_\gamma^{-T}]^T$ with $n \times nr$ matrix $\tilde{X} = [\text{diag}(\tilde{x}_1), \dots, \text{diag}(\tilde{x}_r)]$, and, $L_\gamma = \text{blkdiag}(L_\xi, L_\beta, L_z)$, and, $(2n+p+nr) \times n$ matrix Q is made up of n unit norm orthonormal eigenvectors of $I - H(H^T H)^{-1} H^T$ corresponding to the eigenvalue 1. The discrepancy parameter μ is reparametrized as $q = -Q^T D(\theta) \tilde{\mu}$, where $\tilde{\mu} = (\mu^T, \mu_\gamma^T L_\gamma^{-T})^T$ with $\mu_\gamma = (\mu_\xi^T, \mu_\beta^T, \mu_z^T)^T$ collecting the prior location parameters of γ . The prior shape parameter $\alpha = (\alpha_\epsilon^T, \alpha_\xi^T, \alpha_\beta^T, \alpha_z^T)^T$, and scale parameter $\kappa = (\kappa_\epsilon^T, \kappa_\xi^T, \kappa_\beta^T, \kappa_z^T)^T$ are uniquely determined by the log partition functions in $\psi(h) = (\psi_y(h_1)^T, \psi_\xi(h_2)^T, \psi_\beta(h_3)^T, \psi_z(h_4)^T)^T$ for $h = (h_1, h_2, h_3, h_4) \in \mathbb{R}^{2n+p+nr}$ with $h_1, h_2 \in \mathbb{R}^n$, $h_3 \in \mathbb{R}^p$ and $h_4 \in \mathbb{R}^{nr}$, where all of the log partition functions operate element-wise on the arguments. Then,

$$(\gamma^T, q^T)^T | y \propto \text{GCM}(0_{2n+p+nr}, V, \alpha^*, \kappa^*, D, \pi; \psi),$$

where the posterior shape parameter $\alpha^* = ((y + \alpha_\epsilon)^T, \alpha_\xi^T, \alpha_\beta^T, \alpha_z^T)^T$, and, posterior scale parameter $\kappa^* = ((b + \kappa_\epsilon)^T, \kappa_\xi^T, \kappa_\beta^T, \kappa_z^T)^T$.

Proof. The posterior distribution is derived easily by observing that

$$p((\gamma^T, q^T)^T | y) \propto p(y | (\gamma^T, q^T)^T) \times p((\gamma^T, q^T)^T).$$

Define $H_1 = [I : X : \tilde{X}]$. The observed likelihood can be rewritten as

$$\begin{aligned} p(y | \gamma, \mu) &\propto \exp \left\{ y^T (X\beta + \tilde{X}z + \xi - \mu) - b^T \psi_y(X\beta + \tilde{X}z + \xi - \mu) \right\} \\ &= \exp \left\{ y^T (H_1 \gamma - \mu) - b^T \psi_y(H_1 \gamma - \mu) \right\}. \end{aligned} \quad (\text{A2})$$

Following the definition of the GCM distribution as in (5), we write the joint prior as

$$\begin{aligned} p((\gamma^T, q^T)^T) &\propto \int \exp \left\{ \alpha^T D(\theta)^{-1} \begin{bmatrix} H & Q \end{bmatrix} \begin{bmatrix} \gamma \\ q \end{bmatrix} - \kappa^T \psi \left(D(\theta)^{-1} \begin{bmatrix} H & Q \end{bmatrix} \begin{bmatrix} \gamma \\ q \end{bmatrix} \right) \right\} \pi(\theta) d\theta \\ &= \int \exp \left\{ \alpha^T (D(\theta)^{-1} H \gamma - \tilde{\mu}) - \kappa^T \psi(D(\theta)^{-1} H \gamma - \tilde{\mu}) \right\} \pi(\theta) d\theta \\ &= \int \exp \left\{ (\alpha_\epsilon^T, \alpha_\xi^T, \alpha_\beta^T, \alpha_z^T) \left(D(\theta)^{-1} \begin{bmatrix} H_1 \\ L_\gamma^{-1} \end{bmatrix} \gamma - \begin{bmatrix} \mu \\ L_\gamma^{-1} \mu_\gamma \end{bmatrix} \right) \right. \\ &\quad \left. - (\kappa_\epsilon^T, \kappa_\xi^T, \kappa_\beta^T, \kappa_z^T) \psi \left(D(\theta)^{-1} \begin{bmatrix} H_1 \\ L_\gamma^{-1} \end{bmatrix} \gamma - \begin{bmatrix} \mu \\ L_\gamma^{-1} \mu_\gamma \end{bmatrix} \right) \right\} \pi(\theta) d\theta \\ &= \int \exp \left\{ \alpha_\epsilon^T (H_1 \gamma - \mu) - \kappa_\epsilon^T \psi_y(H_1 \gamma - \mu) \right\} \\ &\quad \times \exp \left\{ \alpha_\gamma^T (D_\gamma(\theta)^{-1} L_\gamma^{-1} \gamma - L_\gamma^{-1} \mu_\gamma) \right. \\ &\quad \left. - \kappa_\gamma^T \psi_\gamma(D_\gamma(\theta)^{-1} L_\gamma^{-1} \gamma - L_\gamma^{-1} \mu_\gamma) \right\} \pi(\theta) d\theta, \end{aligned} \quad (\text{A3})$$

where $\alpha_\gamma = (\alpha_\xi^T, \alpha_\beta^T, \alpha_z^T)^T$, $\kappa_\gamma = (\kappa_\xi^T, \kappa_\beta^T, \kappa_z^T)^T$, and, $D_\gamma(\theta) = \text{blkdiag}(\sigma_\xi I_n, D_\beta(\theta), D_z(\theta))$. The second equality above follows from the fact that $q = -Q^T D(\theta) \tilde{\mu}$, which implies $\tilde{\mu} = -D(\theta)^{-1} Q q$

since $Q^T Q = I$. Multiply (A2) with (A3) to obtain

$$\begin{aligned}
p((\gamma^T, q^T)^T | y, \theta) &\propto \int \exp \{ (y + \alpha_\epsilon)^T (H_1 \gamma - \mu) - (b + \kappa_\epsilon)^T \psi_y (H_1 \gamma - \mu) \} \\
&\quad \times \exp \{ \alpha_\gamma^T (D_\gamma(\theta)^{-1} L_\gamma^{-1} \gamma - L_\gamma^{-1} \mu_\gamma) \\
&\quad - \kappa_\gamma^T \psi_\gamma (D_\gamma(\theta)^{-1} L_\gamma^{-1} \gamma - L_\gamma^{-1} \mu_\gamma) \} \pi(\theta) d\theta \\
&\propto \text{GCM}(0_{2n+p+nr}, V, \alpha^*, \kappa^*, D, \pi; \psi),
\end{aligned} \tag{A4}$$

where $\alpha^* = ((y + \alpha_\epsilon)^T, \alpha_\gamma^T)^T$, and $\kappa^* = ((b + \kappa_\epsilon)^T, \kappa_\gamma^T)^T$. The final step follows from comparing the last line of (A3) with the density of a GCM distribution, as given in the first line of (A3). \square

The main article considers a special case of Theorem A2, with $L_\xi = I_n$ and the location parameters $\mu_\xi = 0_n$ and $\mu_z = 0_{nr}$. Furthermore, we assume $\psi_\xi(\cdot)$, $\psi_\beta(\cdot)$, and $\psi_z(\cdot)$ to be the log-partition functions corresponding to the Gaussian density. This implies that the shape parameters $\alpha_\xi = 0_n$, $\alpha_\beta = 0_n$, $\alpha_z = 0_{nr}$, and the scale parameters $\kappa_\xi = (1/2)1_n$, $\kappa_\beta = (1/2)1_p$, and $\kappa_z = (1/2)1_{nr}$.

A.3. Equivalence with alternative construction. In this section, we establish Theorem A2 as an alternative formulation of the hierarchical model in (7). We essentially show the equivalence of (7) and (8), thus implying that the hierarchical model (7) indeed yields the posterior distribution (9). Instead of a GCM prior jointly on $(\gamma^T, q^T)^T$, model (7) places a GCM_c prior

$$\xi | \beta, z, \mu, \theta \sim \text{GCM}_c(\tilde{\mu}_\xi, H_\xi, \alpha_\xi^*, \kappa_\xi^*, D_\xi, \pi_\xi; \psi_\xi^*) \tag{A5}$$

where $H_\xi = [I_n : L_\xi^{-1}]^T$ is $2n \times n$, location parameter $\tilde{\mu}_\xi = ((\mu - X\beta - \tilde{X}z)^T, L_\xi^{-1} \mu_\xi^T)^T$, shape and scale parameters $\alpha_\xi^* = (\alpha_\epsilon^T, \alpha_\gamma^T)^T$ and $\kappa_\xi^* = (\kappa_\epsilon^T, \kappa_\gamma^T)^T$, respectively. And, $\psi_\xi^*(h) = (\psi_y(h_1)^T, \psi_\xi(h_2)^T)^T$, where $h = (h_1, h_2) \in \mathbb{R}^{2n}$ with $h_1, h_2 \in \mathbb{R}^n$. This yields

$$\begin{aligned}
p(\xi | \beta, z, \mu) &\propto \exp \left\{ (\alpha_\epsilon^T, \alpha_\gamma^T) \left(D_\xi(\theta)^{-1} \begin{bmatrix} I_n \\ L_\xi^{-1} \end{bmatrix} \xi - \begin{bmatrix} \mu - X\beta - \tilde{X}z \\ L_\xi^{-1} \mu_\xi \end{bmatrix} \right) \right. \\
&\quad \left. - (\kappa_\epsilon^T, \kappa_\gamma^T) \psi_\xi^* \left(D_\xi(\theta)^{-1} \begin{bmatrix} I_n \\ L_\xi^{-1} \end{bmatrix} \xi - \begin{bmatrix} \mu - X\beta - \tilde{X}z \\ L_\xi^{-1} \mu_\xi \end{bmatrix} \right) \right\} \\
&= \exp \left\{ (\alpha_\epsilon^T, \alpha_\gamma^T) \left(D_\xi(\theta)^{-1} \begin{bmatrix} I_n & X & \tilde{X} \\ L_\xi^{-1} & 0 & 0 \end{bmatrix} \xi - \begin{bmatrix} \mu \\ L_\xi^{-1} \mu_\xi \end{bmatrix} \right) \right. \\
&\quad \left. - (\kappa_\epsilon^T, \kappa_\gamma^T) \psi_\xi^* \left(D_\xi(\theta)^{-1} \begin{bmatrix} I_n & X & \tilde{X} \\ L_\xi^{-1} & 0 & 0 \end{bmatrix} \xi - \begin{bmatrix} \mu \\ L_\xi^{-1} \mu_\xi \end{bmatrix} \right) \right\}.
\end{aligned} \tag{A6}$$

We assign the same priors on β and z , that is given by

$$\begin{aligned}
p(\beta | \theta) &\propto \exp \{ \alpha_\beta^T (D_\beta(\theta)^{-1} L_\beta^{-1} \beta - L_\beta^{-1} \mu_\beta) - \kappa_\beta^T \psi_\beta (D_\beta(\theta)^{-1} L_\beta^{-1} \beta - L_\beta^{-1} \mu_\beta) \} \\
p(z | \theta) &\propto \exp \{ \alpha_z^T (D_z(\theta)^{-1} L_z^{-1} z - L_z^{-1} \mu_z) - \kappa_z^T \psi_z (D_z(\theta)^{-1} L_z^{-1} z - L_z^{-1} \mu_z) \}.
\end{aligned} \tag{A7}$$

Combine (A8) with the priors of β and z and assign an improper prior on q given by $p(q) \propto 1$. Then the joint prior of $(\gamma^T, q^T)^T$ is same as that of in (7). This can be seen by writing

$$\begin{aligned}
p((\gamma^T, q^T)) &= \int p(\xi \mid \beta, z, \mu, \theta) \times p(\beta \mid \theta) \times p(z \mid \theta) \times p(q) \times \pi(\theta) d\theta \\
&\propto \int \exp \left\{ (\alpha_\epsilon^T, \alpha_\xi^T, \alpha_\beta^T, \alpha_z^T) \left(D(\theta)^{-1} \begin{bmatrix} I_n & X & \tilde{X} \\ L_\xi^{-1} & 0 & 0 \\ 0 & L_\beta^{-1} & 0 \\ 0 & 0 & L_z^{-1} \end{bmatrix} \begin{bmatrix} \xi \\ \beta \\ z \end{bmatrix} - \begin{bmatrix} \mu \\ L_\xi^{-1} \mu_\xi \\ L_\beta^{-1} \mu_\beta \\ L_z^{-1} \mu_z \end{bmatrix} \right) \right. \\
&\quad \left. - (\kappa_\epsilon^T, \kappa_\xi^T, \kappa_\beta^T, \kappa_z^T) \psi \left(D(\theta)^{-1} \begin{bmatrix} I_n & X & \tilde{X} \\ L_\xi^{-1} & 0 & 0 \\ 0 & L_\beta^{-1} & 0 \\ 0 & 0 & L_z^{-1} \end{bmatrix} \begin{bmatrix} \xi \\ \beta \\ z \end{bmatrix} - \begin{bmatrix} \mu \\ L_\xi^{-1} \mu_\xi \\ L_\beta^{-1} \mu_\beta \\ L_z^{-1} \mu_z \end{bmatrix} \right) \right\} \\
&\quad \times \pi(\theta) d\theta \\
&= \int \exp\{\alpha^T (D(\theta)^{-1} H \gamma - \tilde{\mu}) - \kappa^T \psi(D(\theta)^{-1} H \gamma - \tilde{\mu})\} \pi(\theta) d\theta \\
&= \int \exp\{\alpha^T D(\theta)^{-1} (H \gamma + Q q) - \kappa^T \psi(D(\theta)^{-1} (H \gamma + Q q))\} \pi(\theta) d\theta \\
&= \int \exp\{\alpha^T D(\theta)^{-1} V^{-1} (\gamma^T, q^T)^T - \kappa^T \psi(D(\theta)^{-1} V^{-1} (\gamma^T, q^T)^T)\} \pi(\theta) d\theta \\
&\propto \text{GCM}(0_{2n+p+nr}, V, \alpha, \kappa, D, \pi; \psi),
\end{aligned} \tag{A8}$$

which aligns with our specification in (7), thus obtaining its equivalence with (8).

A.4. Multivariate spatial-temporal process. In this section, we outline some results related to the multivariate spatial-temporal process specification. Let $\mathcal{L} = \{\ell_1, \dots, \ell_n\}$ and $\tilde{\mathcal{L}} = \{\tilde{\ell}_1, \dots, \tilde{\ell}_{\tilde{n}}\}$ be two fixed sets of n and \tilde{n} distinct space-time coordinates in \mathcal{D} such that $\mathcal{L} \cap \tilde{\mathcal{L}} = \emptyset$. Following (11), define a $r \times 1$ multivariate spatial-temporal Gaussian process $z(\ell) \sim \mathcal{GP}(0, R(\cdot, \cdot; \theta_{\text{sp}}) \Sigma)$ for some correlation kernel $R(\cdot, \cdot; \theta_{\text{sp}})$. Let $n \times r$ matrix $Z = [z_1 : \dots : z_r]$ and $\tilde{n} \times r$ matrix $\tilde{Z} = [\tilde{z}_1 : \dots : \tilde{z}_r]$ denote the spatial-temporal process at \mathcal{L} and $\tilde{\mathcal{L}}$ respectively. Assume θ_{sp} to be fixed.

Theorem A3. Suppose $[Z^T, \tilde{Z}^T]^T \mid \Sigma \sim \text{MN}_{n+\tilde{n}, r}(0, \tilde{V}_z, \Sigma)$, where $\tilde{V}_z = [(R : C); (C^T, \tilde{R})]$ with $n \times n$ correlation matrix $R = R(\mathcal{L}; \theta_{\text{sp}})$, $\tilde{n} \times \tilde{n}$ correlation matrix $\tilde{R} = R(\tilde{\mathcal{L}}; \theta_{\text{sp}})$, and $C = [R(\ell, \ell'; \theta_{\text{sp}})]$ is $n \times \tilde{n}$ with $\ell \in \mathcal{L}, \ell' \in \tilde{\mathcal{L}}$, all assumed known under a fixed value of θ_{sp} . If $\Sigma \sim \text{IW}(\nu_z + 2r, \Psi)$, then

- (a) posterior distribution $\Sigma \mid Z \sim \text{IW}(n + \nu_z + 2r, Z^T R^{-1} Z + \Psi)$,
- (b) marginal distribution $Z \sim \text{MT}_{n, r}(\nu_z, 0, R, \Psi)$, and,
- (c) posterior predictive $\tilde{Z} \mid Z \sim \text{MT}_{\tilde{n}, r}(\nu_z + n, C^T R^{-1} Z, \tilde{R} - C^T R^{-1} C, Z^T R^{-1} Z + \Psi)$.

Proof. We follow Gupta and Nagar (1999) for definitions of relevant matrix variate distributions used in the following proof. From the distribution of $[Z^T, \tilde{Z}^T]^T$ specified, the marginal distribution of Z conditioned on Σ is $Z \mid \Sigma \sim \text{MN}_{n, r}(0_{n, r}, R, \Sigma)$ which corresponds to the density

$$p(Z \mid \Sigma) = (2\pi)^{-\frac{nr}{2}} |\Sigma|^{-\frac{n}{2}} |R|^{-\frac{r}{2}} \exp \left\{ -\frac{1}{2} \text{tr}(\Sigma^{-1} Z^T R^{-1} Z) \right\}, \tag{A9}$$

where $\text{tr}(\cdot)$ denotes trace of a square matrix. Moreover, the prior $\Sigma \sim \text{IW}(\nu_z + 2r, \Psi)$ has density

$$p(\Sigma) = \frac{|\Psi|^{\frac{1}{2}(\nu_z+r-1)}}{2^{\frac{1}{2}r(\nu_z+r-1)}\Gamma_r(\frac{1}{2}(\nu_z+r-1))} |\Sigma|^{-\frac{1}{2}(\nu_z+2r)} \exp\left\{-\frac{1}{2}\text{tr}(\Sigma^{-1}\Psi)\right\}, \quad (\text{A10})$$

where $\Gamma_r(\cdot)$ denotes the multivariate gamma function (Gupta and Nagar, 1999). From (A9) and (A10), we derive the posterior distribution $p(\Sigma | Z)$ as

$$\begin{aligned} p(\Sigma | Z) &\propto p(Z | \Sigma) \times p(\Sigma) \\ &\propto |\Sigma|^{-\frac{n}{2}} \exp\left\{-\frac{1}{2}\text{tr}(\Sigma^{-1}Z^T R^{-1}Z)\right\} \times |\Sigma|^{-\frac{1}{2}(\nu_z+2r)} \exp\left\{-\frac{1}{2}\text{tr}(\Sigma^{-1}\Psi)\right\} \\ &= |\Sigma|^{-\frac{1}{2}(n+\nu_z+2r)} \exp\left\{-\frac{1}{2}\text{tr}(\Sigma^{-1}(Z^T R^{-1}Z + \Psi))\right\} \\ &\propto \text{IW}(\Sigma | n + \nu_z + 2r, Z^T R^{-1}Z + \Psi). \end{aligned} \quad (\text{A11})$$

The last step follows from comparing the terms up to a proportionality constant with that of a Inverse-Wishart density as given in (A10). This proves statement (a) of Theorem A3. In order to find the marginal distribution of Z , we use the following relation between the marginal, likelihood and the prior densities

$$p(Z) = \frac{p(Z | \Sigma)p(\Sigma)}{p(\Sigma | Z)}.$$

We use the posterior density $p(\Sigma | Z)$ obtained above, and, evaluate

$$\begin{aligned} p(Z) &= (2\pi)^{-\frac{nr}{2}} |\Sigma|^{-\frac{n}{2}} |R|^{-\frac{r}{2}} \exp\left\{-\frac{1}{2}\text{tr}(\Sigma^{-1}Z^T R^{-1}Z)\right\} \\ &\quad \times 2^{-\frac{1}{2}r(\nu_z+r-1)} \Gamma_r\left(\frac{\nu_z+r-1}{2}\right)^{-1} |\Psi|^{\frac{1}{2}(\nu_z+r-1)} |\Sigma|^{-\frac{1}{2}(\nu_z+2r)} \exp\left\{-\frac{1}{2}\text{tr}(\Sigma^{-1}\Psi)\right\} \\ &\quad \times 2^{\frac{1}{2}r(n+\nu_z+r-1)} \Gamma_r\left(\frac{n+\nu_z+r-1}{2}\right) |Z^T R^{-1}Z + \Psi|^{-\frac{1}{2}(n+\nu_z+r-1)} \\ &\quad \times |\Sigma|^{\frac{1}{2}(n+\nu_z+2r)} \exp\left\{\frac{1}{2}\text{tr}(\Sigma^{-1}(Z^T R^{-1}Z + \Psi))\right\} \\ &= (\pi)^{-\frac{nr}{2}} \frac{\Gamma_r(\frac{n+\nu_z+r-1}{2})}{\Gamma_r(\frac{\nu_z+r-1}{2})} |R|^{-\frac{r}{2}} |\Psi|^{\frac{1}{2}(\nu_z+r-1)} |Z^T R^{-1}Z + \Psi|^{-\frac{1}{2}(n+\nu_z+r-1)} \\ &= (\pi)^{-\frac{nr}{2}} \frac{\Gamma_r(\frac{n+\nu_z+r-1}{2})}{\Gamma_r(\frac{\nu_z+r-1}{2})} |R|^{-\frac{r}{2}} |\Psi|^{\frac{1}{2}(\nu_z+r-1)} |\Psi|^{-\frac{1}{2}(\nu_z+n+r-1)} \\ &\quad \times |I_r + \Psi^{-1}Z^T R^{-1}Z|^{-\frac{1}{2}(\nu_z+n+r-1)} \\ &= (\pi)^{-\frac{nr}{2}} \frac{\Gamma_r(\frac{n+\nu_z+r-1}{2})}{\Gamma_r(\frac{\nu_z+r-1}{2})} |R|^{-\frac{r}{2}} |\Psi|^{-\frac{n}{2}} |I_r + \Psi^{-1}Z^T R^{-1}Z|^{-\frac{1}{2}(\nu_z+n+r-1)} \\ &= \text{MT}_{n,r}(Z | \nu_z, 0, R, \Sigma), \end{aligned} \quad (\text{A12})$$

where $\text{MT}_{n,r}(Z | \nu_z, 0, R, \Sigma)$ corresponds to the density of $n \times r$ matrix variate t -distribution with degrees of freedom ν_z , location parameter $0_{n,r}$, $n \times n$ between-rows covariance matrix R , $r \times r$ between-columns covariance matrix, evaluated at Z . This completes the proof of statement (b).

To prove the statement (c), we proceed with joint distribution of Z and \tilde{Z} conditioned on Σ . Consider the Cholesky decomposition of the random variable $\Sigma = L_\Sigma L_\Sigma^\top$. Conditioned on Σ , we transform the matrix variate $[Z^\top, \tilde{Z}^\top]^\top$ by multiplying $L_\Sigma^{-\top}$ on the right. This yields the distribution of the transformed $(n + \tilde{n}) \times r$ random matrix $[L_\Sigma^{-1}Z^\top, L_\Sigma^{-1}\tilde{Z}^\top]^\top \sim \text{MN}_{n+\tilde{n},r}(0, \tilde{V}_z, I_r)$. This follows from properties on linear transformation of matrix normal variates and the identity $L_\Sigma^{-1}\Sigma L_\Sigma^{-\top} = L_\Sigma^{-1}L_\Sigma L_\Sigma^\top L_\Sigma^{-\top} = I_r$. This implies that this transformation has made the columns to be independent. We use the result on conditional multivariate Gaussian distribution independently on the columns of the transformed matrix random variable and then combine them, to obtain

$$\begin{aligned} \tilde{Z}L_\Sigma^{-\top} \mid Z, \Sigma &\sim \text{MN}_{\tilde{n},r} \left(C^\top R^{-1}ZL_\Sigma^{-\top}, \tilde{R} - C^\top R^{-1}C, I_r \right) \\ \iff \tilde{Z} \mid Z, \Sigma &\sim \text{MN}_{\tilde{n},r} \left(C^\top R^{-1}Z, \tilde{R} - C^\top R^{-1}C, \Sigma \right), \end{aligned} \quad (\text{A13})$$

which follows from multiplying by L_Σ^\top on the right which transforms the location to $C^\top R^{-1}Z = C^\top R^{-1}ZL_\Sigma^{-\top}L_\Sigma^\top$, and changes the between-row covariance matrix to $L_\Sigma I_r L_\Sigma^\top = \Sigma$. Now, in order to obtain the conditional distribution $p(\tilde{Z} \mid Z)$, we need to integrate out Σ as follows

$$p(\tilde{Z} \mid Z) = \int p(\tilde{Z} \mid Z, \Sigma) p(\Sigma \mid Z) d\Sigma.$$

From (a), we know that the posterior distribution $\Sigma \mid Z \sim \text{IW}(n + \nu_z + 2r, Z^\top R^{-1}Z + \Psi)$. We use the result of the same integral in (b), and plug in $n + \nu_z$ in place of ν_z , and $Z^\top R^{-1}Z + \Psi$ in place of Ψ , to obtain the marginal distribution $p(\tilde{Z} \mid Z)$ as a matrix variate t -distribution

$$\tilde{Z} \mid Z \sim \text{MT}_{\tilde{n},r}(n + \nu_z, C^\top R^{-1}Z, \tilde{R} - C^\top R^{-1}C, Z^\top R^{-1}Z + \Psi).$$

This completes the proof of the statement (c) of Theorem A3. \square

A.5. Posterior sampling of scale parameters. The projection expression (13) in the main article is required to sample the fixed effects β and the random effects z from the marginal model (8), obtained by integrating out the scale parameters σ_β^2 and θ_z , respectively. Once we have obtained posterior samples $\{\beta^{(b)}, z^{(b)}\}$ from the posterior distribution (9), posterior samples of the scale parameters can be obtained easily. Note that, we need samples of σ_β^2 and θ_z from their marginal posterior $p(\sigma_\beta^2, \theta_z \mid y, M)$ which can be rewritten as

$$\begin{aligned} p(\sigma_\beta^2, \theta_z \mid y, M) &= \int p(\sigma_\beta^2, \theta_z \mid \beta, z, y, M) p(\beta, z \mid y, M) d\beta dz \\ &= \int p(\sigma_\beta^2, \theta_z \mid \beta, z, M) p(\beta, z \mid y, M) d\beta dz \\ &= \int p(\sigma_\beta^2 \mid \beta, M) p(\theta_z \mid z, M) p(\beta, z \mid y, M) d\beta dz, \end{aligned} \quad (\text{A14})$$

where the penultimate step follows from the fact that both the scale parameters σ_β^2 and θ_z are conditionally independent of the data y , given β, z and the fixed hyperparameters in M . The last step follows from the fact that σ_β^2 is independent of θ_z and z given β and M , which follows from the independent prior specification of β, z and their corresponding scale parameters. Hence, given posterior samples $\{\beta^{(b)}, z^{(b)}\}$ from $p(\beta, z \mid y, M)$, for each $\beta^{(b)}$, we need to sample $\sigma_\beta^{2(b)} \sim p(\sigma_\beta^2 \mid \beta^{(b)}, M)$, and, for each sample of $z^{(b)}$, we need to sample $\theta_z^{(b)} \sim p(\theta_z \mid z^{(b)}, M)$. Thus, the

posterior samples $\{\beta^{(b)}, z^{(b)}, \sigma_{\beta}^{2(b)}, \theta_z^{(b)}\}$ will represent samples from the joint posterior distribution $p(\beta, z, \sigma_{\beta}^2, \theta_z | y, M)$. Thus, choosing conditionally conjugate priors for the scale parameters (e.g., inverse-gamma/inverse-Wishart) plays a key role in conveniently sampling them from the joint posterior distribution.

Since, we place a multivariate Gaussian prior $\beta | \sigma_{\beta}^2, M \sim \mathbf{N}(\mu_{\beta}, \sigma_{\beta}^2 V_{\beta})$ along with an inverse-gamma prior $\sigma_{\beta}^2 \sim \text{IG}(\nu_{\beta}/2, \nu_{\beta}/2)$, we derive the conditional posterior distribution of σ_{β}^2 as

$$p(\sigma_{\beta}^2 | \beta^{(b)}, M) = \text{IG} \left(\sigma_{\beta}^2 \left| \frac{\nu_{\beta} + p}{2}, \frac{\nu_{\beta} + Q_1(\beta^{(b)}; M)}{2} \right. \right), \quad (\text{A15})$$

where $Q_1(v; M) = (v - \mu_{\beta})^T V_{\beta}^{-1} (v - \mu_{\beta})$ for any $v \in \mathbb{R}^p$. Note that, the hyperparameters μ_{β} and V_{β} are specified by M . Similarly, under the independent process model, we derive

$$p(\theta_z | z^{(b)}, M) = \prod_{j=1}^r p(\sigma_{z_j}^2 | z_j^{(b)}, M),$$

where $\theta_z = \{\sigma_{z_j}^2 : j = 1, \dots, r\}$. This follows from the assumption of independent process $z_j(\ell)$ and independent prior on each $\sigma_{z_j}^2$ for $j = 1, \dots, r$. Under assumption of the prior distribution $\sigma_{z_j}^2 \sim \text{IG}(\nu_{z_j}/2, \nu_{z_j}/2)$ for each j , we have

$$p(\sigma_{z_j}^2 | z^{(b)}, M) = \text{IG} \left(\sigma_{z_j}^2 \left| \frac{\nu_{z_j} + n}{2}, \frac{\nu_{z_j} + Q_{2j}(z_j^{(b)}; M)}{2} \right. \right), \quad j = 1, \dots, r, \quad (\text{A16})$$

where $Q_{2j}(v; M) = v^T R(\theta_{\text{sp},j}) v$ for any $v \in \mathbb{R}^n$ and $j = 1, \dots, r$. Here, the process parameters $\theta_{\text{sp},j}$ for each j are specified by M . Under the multivariate process specification with inverse-Wishart prior $\Sigma \sim \text{IW}(\nu_z + 2r, \Psi)$, we use Theorem A3 in order to obtain $p(\theta_z | z^{(b)}, M) = p(\Sigma | z^{(b)}, M)$ as

$$p(\Sigma | z^{(b)}, M) = \text{IW} \left(\Sigma \left| n + \nu_z + 2r, Q_3(z^{(b)}; M) \right. \right), \quad (\text{A17})$$

where $Q_3(v; M) = \Psi + V^T R(\theta_{\text{sp}})^{-1} V$, with $V \in \mathbb{R}^{n \times r}$ such that $\text{vec}(V) = v$, for any $v \in \mathbb{R}^{nr}$. Here, the process parameters θ_{sp} and the scale matrix Ψ are specified by M .

APPENDIX B. COMPUTATIONAL DETAILS

In this section, we present an overview of the algorithms that we have developed to implement our proposed methodology in a computationally efficient way. We achieve this through optimizing linear algebraic operations by avoiding unnecessary expensive matrix operations that are slow and careful utilization of sparsity and other structural properties of matrices.

B.1. Computationally efficient algorithm for projection. The projection expression (13) is necessary to compute in order to obtain posterior samples of $\gamma = (\xi^T, \beta^T, z^T)^T$. Note that, it involves computing the inverse of the $(n+p+nr) \times (n+p+nr)$ matrix $H^T H$, where $H = [(I_n : X : \tilde{X}^T, L_{\gamma}^{-T})]^T$. We proceed by first computing different submatrices of $(H^T H)^{-1}$ and keeping it stored so that it can be reused whenever we need to find the projection for each $v^{(b)}$. We partition $H^T H$ as

$$H^T H = \begin{bmatrix} 2I_n & X & \tilde{X} \\ X^T & X^T X + V_{\beta}^{-1} & X^T \tilde{X} \\ \tilde{X}^T & \tilde{X}^T X & \tilde{X}^T \tilde{X} + V_z^{-1} \end{bmatrix} = \begin{bmatrix} A & B^T \\ B & D \end{bmatrix}, \quad D = \begin{bmatrix} A_1 & B_1^T \\ B_1 & D_1 \end{bmatrix}, \quad (\text{A18})$$

where $V_\beta = L_\beta L_\beta^\top$, $V_z = L_z L_z^\top$, $n \times n$ matrix $A = 2I_n$, $(p + nr) \times n$ matrix $B = [X : \tilde{X}]^\top$, and $(p + nr) \times (p + nr)$ matrix D is further partitioned into $p \times p$ matrix $A_1 = X^\top X + V_\beta^{-1}$, $nr \times p$ matrix $B_1 = \tilde{X}^\top X$, and $nr \times nr$ matrix $D_1 = \tilde{X}^\top \tilde{X} + V_z^{-1}$. It suffices to develop the algorithm as computing $(H^\top H)^{-1}v$ for any $v \in \mathbb{R}^{n+p+nr}$. Rewrite v as $v = (v_1^\top, v_2^\top)^\top$ where v_1 is $n \times 1$ and v_2 is $(p + nr) \times 1$. Then, $(H^\top H)^{-1}v$ can be computed using

$$(H^\top H)^{-1}v = \begin{bmatrix} S_A^{-1}(v_1 - B^\top D^{-1}v_2) \\ D^{-1}v_2 - D^{-1}BS_A^{-1}(v_1 - B^\top D^{-1}v_2) \end{bmatrix}, \quad (\text{A19})$$

where $S_A = A - B^\top D^{-1}B$ denotes the Schur complement of the submatrix A of $H^\top H$. Note that, computing D^{-1} plays a central role in evaluating the projection (A19). Similarly, we find $D^{-1}B$ as

$$D^{-1}B = D^{-1} \begin{bmatrix} X^\top \\ \tilde{X}^\top \end{bmatrix} = \begin{bmatrix} S_{A_1}^{-1}(X - \tilde{X}D_1^{-1}\tilde{X}^\top X)^\top \\ D_1^{-1}(\tilde{X}^\top - \tilde{X}^\top X S_{A_1}^{-1}(X - \tilde{X}D_1^{-1}\tilde{X}^\top X)^\top) \end{bmatrix}, \quad (\text{A20})$$

where $S_{A_1} = A_1 - B_1^\top D_1^{-1}B_1$, $D_1 = \tilde{X}^\top \tilde{X} + V_z^{-1}$ and $B_1 = \tilde{X}^\top X$. Here, the computational bottleneck lies in inverting D_1 , which essentially involves two inversions of $nr \times nr$ matrices when approached naively i.e., $(\tilde{X}^\top \tilde{X} + V_z^{-1})^{-1}$. Here, we use the Sherman-Morrison-Woodbury identity

$$D_1^{-1} = V_z - V_z \tilde{X}^\top (I + \tilde{X}V_z \tilde{X}^\top)^{-1} \tilde{X}V_z, \quad (\text{A21})$$

which essentially boils down to inverting the $n \times n$ matrix $I + \tilde{X}V_z \tilde{X}^\top$, which is also known as the capacitance matrix in context of the Sherman-Morrison-Woodbury identity, thus avoiding finding Cholesky decomposition of a $nr \times nr$ matrix. The computation associated with evaluating the projection is dominated by the Cholesky factorization of the capacitance matrix which takes $O(n^3)$ flops. Moreover, computing $\tilde{X}V_z \tilde{X}^\top$ poses as a challenge since the matrix product $V_z \tilde{X}^\top$ requires $O(rn^3)$ floating point operations (flops). We make use of both facts that V_z is block-diagonal and \tilde{X} is sparse and have a particular structure, since $\tilde{X} = [\text{diag}(\tilde{x}_1), \dots, \text{diag}(\tilde{x}_r)]$. Once we have calculated D_1^{-1} , we successively find $D_1^{-1}B_1$, S_{A_1} , $D^{-1}B$ and S_A^{-1} . We compute these quantities only once, and use them for each iteration for sampling $\gamma^{(b)}$ for each b .

B.2. Efficient Cholesky factor updates. We utilize a block Givens rotation algorithm (Golub and Van Loan, 2013, Section 5.1.8) for faster model evaluation during cross-validation. Our algorithm can be regarded as a block-level variant of Kim et al. (2002). Following the setup preceding Algorithm A2, suppose the k th block $\chi_{[k]}$ for each k contains adjacent indices of the data χ . Moreover, suppose evaluating a model needs Cholesky decomposition of a $n \times n$ positive-definite matrix R , where n is the number of observations in χ . In the context of (7), R may correspond to the correlation matrix of a spatial-temporal process. Suppose we have evaluated the model on the full data, and we have stored L , the upper triangular Cholesky factor of R . The consecutive indices of the partitioned data creates K^2 submatrices partitioning R and its upper triangular Cholesky factor L as,

$$R = \begin{bmatrix} R_{11} & R_{21}^\top & \cdots & R_{K1}^\top \\ R_{21} & R_{22} & \cdots & R_{K2}^\top \\ \vdots & \vdots & \ddots & \vdots \\ R_{K1} & R_{K2} & \cdots & R_{KK} \end{bmatrix}, \quad L = \begin{bmatrix} L_{11} & L_{12} & \cdots & L_{1K} \\ 0 & L_{22} & \cdots & L_{2K} \\ \vdots & \vdots & \ddots & \vdots \\ 0 & 0 & \cdots & L_{KK} \end{bmatrix}.$$

Algorithm A1 Fast Cholesky updates of row-deletion using block Givens rotation.

```

1: Input:  $R, L, k$ ; full matrix, its upper-triangular Cholesky factor, block to be deleted
2: Output:  $L_{-k}$ , the Cholesky factor of  $R_{-k}$ , the matrix with  $k$ th block deleted
3: function CHOLESKYCV( $R, L, k$ )
4:   if  $k = 1$  then
5:      $L_{-k} \leftarrow \text{chol}(R_{-k})$ 
6:   else
7:     if  $1 < k < K$  then
8:        $C_{11}^k \leftarrow L_{11}^k$  (pre-computed)
9:        $C_{13}^k \leftarrow L_{13}^k$  (pre-computed)
10:       $C_{33}^k \leftarrow \text{chol}(L_{33}^{kT} L_{33}^k + L_{23}^{kT} L_{23}^k)$ 
11:    else
12:       $L_{-k} =$  upper left  $(K - 1) \times (K - 1)$  submatrices of  $L$  (pre-computed)
13:    return  $L_{-k}$ 

```

For each k such that $1 < k < K$, consider the following representation of the matrices R, L, R_{-k} , the matrix corresponding to $\chi_{[-k]}$ and its upper triangular Cholesky factor L_{-k} .

$$R = \begin{bmatrix} R_{11}^k & R_{21}^{kT} & R_{31}^{kT} \\ R_{21}^k & R_{22}^k & R_{32}^{kT} \\ R_{31}^k & R_{32}^k & R_{33}^k \end{bmatrix}, \quad L = \begin{bmatrix} L_{11}^k & L_{12}^k & L_{13}^k \\ 0 & L_{22}^k & L_{23}^k \\ 0 & 0 & L_{33}^k \end{bmatrix}, \\
R_{-k} = \begin{bmatrix} R_{11}^k & R_{31}^{kT} \\ R_{31}^k & R_{33}^k \end{bmatrix}, \quad L_{-k} = \begin{bmatrix} C_{11}^k & C_{13}^k \\ 0 & C_{33}^k \end{bmatrix},$$

where $R_{22}^k = R_{kk}$. Then, Algorithm A1 finds L_{-k} for each $k = 1, \dots, K$. In Algorithm A1, note that, no computation is needed to find L_{-K} and C_{11}^k, C_{13}^k for $1 < k < K$.

It is worth remarking that the ‘naive approach’ for obtaining L_{-k} involves Cholesky decomposition of R_k for each k , and, hence, requiring $K^{-2}(K - 1)^3 n^3 / 3$ floating point operations (flops). On the other hand, the time complexity of Algorithm A1 is of order

$$\sum_{k=1}^K \left(1 - \frac{k}{K}\right)^3 \frac{n^3}{3} = \frac{n^3}{3K^3} \sum_{k=1}^{K-1} i^3 = \frac{n^3}{3K^3} \frac{K^2(K-1)^2}{4} = \frac{(K-1)^2 n^3}{4K} \frac{1}{3},$$

where the penultimate step follows from the sum of cubes of natural numbers. Hence, we show that Algorithm A1 is theoretically $4(K - 1)/K$ times faster than the naive approach. If $K = 10$ (Vehtari and Lampinen, 2002), then Algorithm A1 theoretically offers approximately 72% efficiency in time complexity over the naive approach. However, it must be noted that modern linear algebra libraries are highly vectorised and are often multithreaded. Hence, it is difficult to accurately translate these purely theoretical flop counts to actual wall clock time. Nevertheless, Algorithm A1 is more efficient than the naive approach.

B.3. Stacking algorithm. Lastly, we detail the algorithm for implementing our proposed stacking framework utilising the aforementioned algorithms. Algorithm A2 outlines the steps required for

Algorithm A2 Predictive stacking algorithm for spatial-temporal GLM

```

1: Input:  $y, X, \tilde{X}, \mathcal{L}, N_s, S, \mathcal{M}, K$ 
2: Output: Posterior samples for each model in  $\mathcal{M}$ , optimal stacking weights  $\hat{w}$ 
3: function STVCGLMSTACK( $y, X, \tilde{X}, \mathcal{L}, N, B, \mathcal{M}, K$ )
4:   Partition the data  $\chi$  into  $K$  blocks  $\chi_{[1]}, \dots, \chi_{[K]}$ .
5:   for  $g = 1$  to  $g = G$  do in parallel
6:     Fit model  $M_g$  on  $\chi$  and obtain posterior samples  $\{\beta_g^{(b)}, z_g^{(b)}\}_{b=1}^{N_s}$  using (14)
7:     for  $k = 1$  to  $k = K$  do
8:       Obtain updated Cholesky factor using choleskyCV( $\cdot, \cdot, k$ ).
9:       Fit model  $M_g$  on  $\chi_{[-k]}$  and obtain samples  $\{\beta_{k,g}^{(s)}, z_{k,g}^{(s)}\}_{s=1}^S$  using (14)
10:      for  $s = 1$  to  $s = S$  do
11:        Use (16) to predict  $\tilde{z}_{k,g}^{(s)}$  at  $\mathcal{L}_{[k]}$  from  $z_{k,g}^{(s)}$ 
12:        Use (19) to find  $p(y(\ell_i) | y_{-i}, M_g), \forall \ell_i \in \mathcal{L}_{[k]}$ 
13:      Optimise (18) to obtain optimal stacking weights  $\hat{w}$ 
14:    return Optimal model weights  $\hat{w}, \{\beta_g^{(b)}, z_g^{(b)}\}_{b=1}^{N_s}$  for  $g = 1, \dots, G$ 

```

estimating the spatially-temporally varying coefficients model (7) in the main article. The inputs X and \tilde{X} in Algorithm A2 correspond to the design matrices appearing in (7), \mathcal{L} denotes spatial-temporal locations, $\mathcal{M} = \{M_1, \dots, M_G\}$ denotes the collection of G candidate models, N_s denotes number of samples to be drawn from each of these G posterior distributions, S denotes the number of samples to be drawn for evaluating the leave-one-out predictive densities as described in (19), and K denotes the number of folds for cross-validation required for fast evaluation of leave-one-out predictive densities. Following a random permutation of the entire dataset, we construct a partition using consecutive indices of the permuted data. This step significantly accelerates evaluation of Cholesky factors using block Givens rotation (Golub and Van Loan, 2013) required during the cross-validation step detailed in Algorithm A1. After partitioning the data, which is denoted by $\chi = (y, X, \tilde{X}, \mathcal{L})$ into K blocks, each block is denoted by $\chi_{[k]}$ and the data with the k th block deleted is denoted by $\chi_{[-k]}$ for $k = 1, \dots, K$. Algorithm A2 is written in a richer and more general context and can be easily adapted to spatial, spatial-temporal, spatially and spatially-temporally varying coefficients models.

APPENDIX C. ADDITIONAL DETAILS ON SIMULATION EXPERIMENTS

C.1. Predictive accuracy. We present some additional results from the simulation experiments carried out in Section 5 of the main article. Analogous to the main article, we evaluate predictive performance of our proposed methods using four simulated datasets each of sample size n , with spatial coordinates sampled uniformly inside the unit square $[0, 1]^2$ and temporal coordinates sampled uniformly within $[0, 1]$. The simulated datasets are based on the natural parameter $\eta(\ell) = x(\ell)^\top \beta + x(\ell)^\top z(\ell)$. For the first two simulated datasets, we simulate the responses as binomial count data with responses $y(\ell) \sim \text{Binomial}(m(\ell), \pi(\ell))$ with $m(\ell)$, the number of trials sampled independently from a Poisson distribution with mean 20 and probability of success

True Process	Model	Method	Sample size (n)				
			$n = 100$	$n = 200$	$n = 300$	$n = 400$	$n = 500$
Multivariate	Multivariate	Stacking	-3.76	-3.64	-3.59	-3.47	-3.41
		MCMC	-3.67	-3.55	-3.49	-3.39	-3.34
	Independent	Stacking	-3.90	-3.86	-3.76	-3.69	-3.56
		MCMC	-3.79	-3.75	-3.68	-3.57	-3.49
Independent	Multivariate	Stacking	-3.68	-3.61	-3.53	-3.47	-3.39
		MCMC	-3.78	-3.72	-3.69	-3.64	-3.62
	Independent	Stacking	-3.79	-3.76	-3.72	-3.52	-3.38
		MCMC	-3.63	-3.56	-3.49	-3.38	-3.34

TABLE A1. Predictive performance of stacking and MCMC under correct and misspecified spatial-temporal models on binomial count data. All values correspond to mean log-pointwise predictive density (MLPD) at $n_h = 100$ held-out locations, based on 5 replications.

$\pi(\ell) = \text{ilogit}(\eta(\ell))$ with $\text{ilogit}(t) = \exp(t)/(1 + \exp(t))$, $t \in \mathbb{R}$ and $\beta = (1, -0.5)$. For the remaining two datasets, we simulate the responses as binary data with responses $y(\ell) \sim \text{Bernoulli}(\pi(\ell))$ with probability of success $\pi(\ell)$ is as defined above. We set $\tilde{x}(\ell) = x(\ell)$, deeming all covariates to have spatially-temporally varying coefficients. Under the independent process assumption, $z_j(\ell) \sim \mathcal{GP}(0, \sigma_{z_j}^2 R_j(\cdot, \cdot))$ for $j = 1, 2$ with $\sigma_{z_1}^2 = 0.25$, $\sigma_{z_2}^2 = 0.5$ and, $(\phi_{11}, \phi_{21}) = (0.5, 2)$ and, $(\phi_{12}, \phi_{22}) = (1, 4)$. For the multivariate case, we assume $\Sigma = [(2, 0.5)^\top, (0.5, 2)^\top]^\top$ and $\phi_1 = 1$ and $\phi_2 = 2$. The choice of β in each simulated data is such that the generated data do not contain excessive zeros. The simulation experiments are conducted with n varying from 200 to 600 with a randomly chosen holdout sample of size $n_h = 100$ over a set of coordinates \mathcal{L}_h . We present the results in Tables A1 and A2.

C.2. Weak identifiability of process parameters. Consider the simulated Poisson count data under the spatially-temporally varying coefficient model (7) as described in Section 5.1. Figure A1 presents the posterior distributions of the process parameters that characterise the two spatial-temporal processes z_1 and z_2 , corresponding to the intercept (ϕ_{11} and ϕ_{21}) and the predictor (ϕ_{21} and ϕ_{22}) respectively, obtained by MCMC (see Section 5.2). None of the process parameters in Fig. A1 have concentrated around their corresponding true values, illustrating their weak identifiability. We also notice similarity in the posterior distributions of the temporal decay parameters ϕ_{11} and ϕ_{12} for both the processes z_1 and z_2 respectively. The same phenomenon is noticed in the posterior distributions of the spatial decay parameters ϕ_{21} and ϕ_{22} . This between-process similarity in the posterior learning of the process parameters justifies the tenability of the “reduced” model that uses common spatial-temporal process parameters across all the r processes in (7). This reduces

True Process	Model	Method	Sample size (n)				
			$n = 100$	$n = 200$	$n = 300$	$n = 400$	$n = 500$
Multivariate	Multivariate	Stacking	-4.36	-4.29	-4.19	-4.07	-3.89
		MCMC	-4.16	-4.11	-4.06	-3.96	-3.81
	Independent	Stacking	-4.41	-4.36	-4.23	-4.19	-4.01
		MCMC	-4.29	-4.21	-4.14	-4.09	-3.94
Independent	Multivariate	Stacking	-4.38	-4.31	-4.22	-4.11	-4.04
		MCMC	-4.24	-4.19	-4.13	-4.06	-3.99
	Independent	Stacking	-4.41	-4.35	-4.27	-4.16	-4.11
		MCMC	-4.26	-4.20	-4.11	-4.07	-3.99

TABLE A2. Predictive performance of stacking and MCMC under correct and misspecified spatial-temporal models on binary data. All values correspond to mean log-pointwise predictive density (MLPD) at $n_h = 100$ held-out locations, based on 5 replications.

the parameter space by r folds. The reduced model further effectuates a substantial decrease in the number of candidate models required for the proposed stacking algorithm.

Moreover, in addition to Fig. 1 in the main article, where we plot the posterior medians of the spatial-temporal random effects for the simulated Poisson count data, Figure A2 plots 100 quantiles of the combined posterior samples of spatial-temporal random effects obtained by stacking against quantiles obtained from MCMC. This demonstrates strong agreement between the posterior distributions obtained from the competing algorithms with most of the points concentrated along the $y = x$ line (red dashed).

We also present results from an additional simulation experiment that demonstrates posterior learning of a random field modelling the underlying spatial or spatial-temporal processes. For convenient visualisation of the random field, we consider spatial data instead of spatial-temporal data in a continuous time domain. We simulate a dataset with responses distributed as $y(s) \sim \text{Poisson}(\exp(x(s)^T \beta + z(s)))$ with sample size 1000. The locations are sampled uniformly inside the unit square $[0, 1]^2$. The explanatory vector $x(s)$ consists of an intercept and one predictor sampled from the standard normal distribution and the regression coefficients are taken as $\beta = (5, -0.5)$. The latent spatial process $z(s) \sim \mathcal{GP}(0, \sigma_z^2 R(\cdot, \cdot; \phi, \nu))$ is a zero-centred Gaussian process with $\sigma_z^2 = 0.4$, $\phi = 3.5$ and $\nu = 0.5$, where $R(\cdot, \cdot; \phi, \nu)$ is the Matérn correlation function,

$$R(s, s'; \phi, \nu) = \frac{(\phi |s - s'|)^\nu}{2^{\nu-1} \Gamma(\nu)} K_\nu(\phi |s - s'|), \quad (\text{A22})$$

$|s - s'|$ is the Euclidean distance between s and s' , and $\theta_{\text{sp}} = \{\phi, \nu\}$. The parameter $\nu > 0$ controls the smoothness of the realised random field, ϕ is the spatial decay parameter, $\Gamma(\cdot)$ denotes the gamma function, and K_ν is the modified Bessel function of the second kind of order ν (Abramowitz

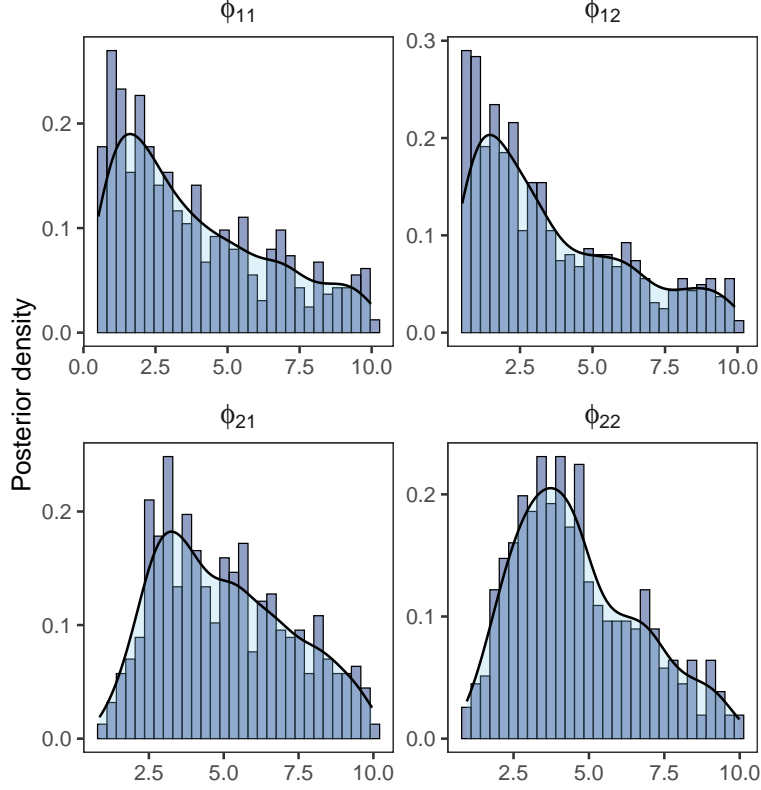


FIGURE A1. Histograms of posterior samples of the spatial-temporal process parameters obtained by MCMC on a fully Bayesian model under the independent process assumption on a simulated Poisson count data of sample 100.

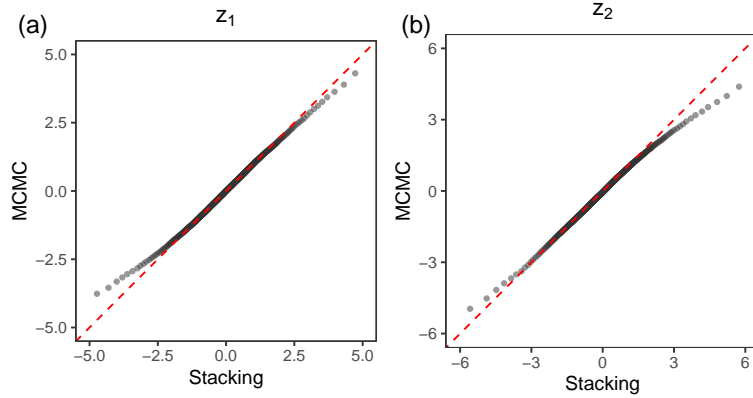


FIGURE A2. Plot of quantiles of the posterior distributions of the spatial-temporal random effects corresponding to (a) intercept and, (b) predictor obtained by stacking against MCMC with the $y = x$ reference as a red dashed line.

and Stegun, 1965, Chapter 10). The model in (7) can be modified for accommodating a spatial regression by considering $r = 1$ and subsequently $\tilde{X} = I_n$. Here, \mathcal{S} is the domain of interest. We stack on the parameters $\Delta = \{\alpha_\epsilon, \sigma_\xi, \phi, \nu\}$ with hyperparameters $\nu_\beta = \nu_z = 3$. We also implement a fully

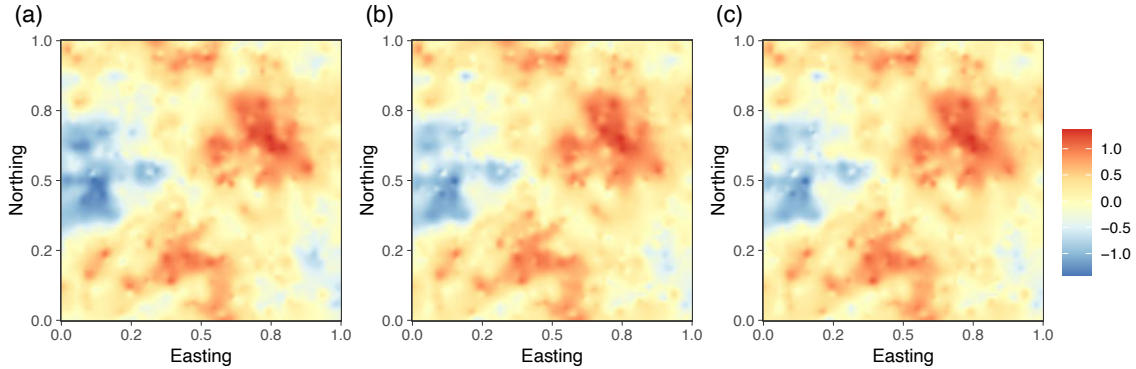


FIGURE A3. Comparison of interpolated surfaces of (a) the true spatial effects, with posterior median of spatial effects obtained by (b) MCMC, and, (c) our proposed predictive stacking algorithm on a simulated spatial count data.

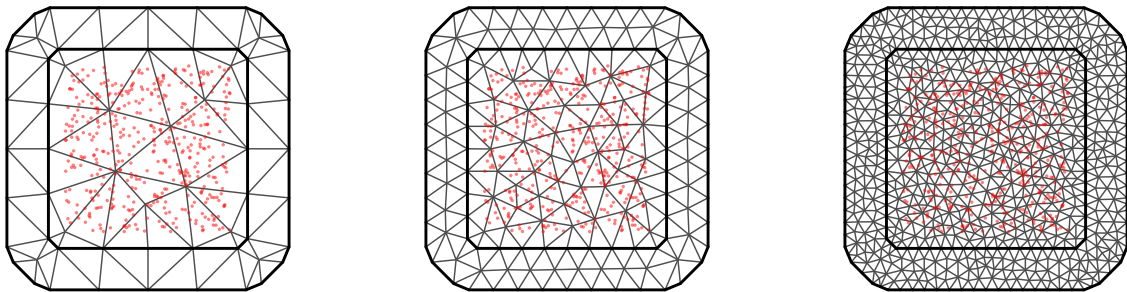


FIGURE A4. Spatial discretization at varying mesh resolutions constructed using INLA, with maximum edge lengths set to 0.5 (left), 0.25 (middle), and 0.15 (right). The 500 training and test locations are overlaid in red.

Bayesian model with uniform priors $U(0.5, 10)$ for ϕ and $U(0.1, 2)$ for ν . We modify our adaptive Metropolis-within-Gibbs algorithm accordingly. Figure A3 compares the posterior distributions of the spatial random effects obtained by predictive stacking and MCMC with its true values. We observe indistinguishable spatial surfaces of the posterior medians of the spatial random effects.

C.3. Additional details on comparison with INLA. Figure A4 illustrates the spatial discretization used in our INLA experiments, showing meshes constructed with varying maximum edge lengths $s_{\text{grid}} \in 0.5, 0.25, 0.15$ and overlaid training and test locations (in red). We set the discrepancy parameter μ to zero, reducing the model to a traditional Poisson regression that is compatible with the INLA framework Rue et al. (2009). After constructing the spatial and temporal meshes, we specified the spatial-temporal processes and defined priors for their hyperparameters using the `stModel.define()` function from `INLAspacetime`. The SPDE projection matrix that links the latent process on the mesh to the observation locations was then constructed using `inla.spde.make.A()`, incorporating both observed and unobserved locations. We fitted the model through the `cgeneric` interface of INLA, and subsequently used `inla.posterior.sample()` to draw samples from the approximate posterior distribution of the latent process and hyperparameters.

	Median	2.5%	97.5%
σ_{11}	0.371	0.170	1.231
σ_{22}	0.077	0.0428	0.214
σ_{33}	0.134	0.351	1.397
ρ_{12}	-0.045	-0.304	0.162
ρ_{13}	-0.487	0.197	0.731
ρ_{23}	-0.343	-0.055	0.184

TABLE A3. North American Breeding Bird Survey (2010-19): Posterior summary (95% credible intervals) of elements of the between-process covariance matrix $\Sigma = ((\sigma_{ij}))$ with $\rho_{ij} = \sigma_{ij}/\sqrt{\sigma_{ii}\sigma_{jj}}$ denoting the correlation between the i th and j th processes in the varying coefficients. 2.5% and 97.5% represent quantiles.

Using these samples together with the projection matrix, we recovered the posterior samples of the latent spatial-temporal process at the observed locations and generated predictions at held out sites. Finally, we computed the mean log pointwise predictive density (MLPD) at the held-out locations to assess predictive performance and compared total runtimes with those obtained from our predictive stacking approach.

APPENDIX D. ADDITIONAL DATA ANALYSIS

We offer some additional data analysis from the North American Breeding Bird Survey to supplement the results in Section 6 of the main article. In the survey, the data are collected annually during the breeding season, primarily in June, along thousands of randomly established roadside survey routes in the United States and Canada. Routes are roughly 24.5 miles (39.2 km) long with counting locations placed at approximately half-mile (800 m) intervals, for a total of 50 stops. At each stop, a citizen scientist, highly skilled in avian identification, conducts a 3-minute point count recording all birds seen within a quarter-mile (400 m) radius and all birds heard. Routes are sampled once per year. In addition to avian count data, this dataset also contains route location information including country, state and the geographic coordinates of the route start point. The variable ‘car’ records the total number of motorised vehicles passing a particular point count stop during the 3-minute count period. The variable ‘noise’ represents the presence/absence of excessive noise defined as noise from sources other than vehicles passing the survey point (e.g. from streams, construction work, vehicles on nearby roads, etc.) lasting 45 seconds that significantly interferes with the observer’s ability to hear birds at the stop during the 3-minute count period. More information on the survey can be found online at BBS 2022 data release (<https://www.usgs.gov/data/2022-release-north-american-breeding-bird-survey-dataset-1966-2021>).

The main article discusses the global regression coefficients under different models. In Table A3, we present the posterior summary of the elements of the between-process covariance matrix under the multivariate process assumption. Figures A5 and A6 display side-by-side plots of the observed point counts and interpolated spatial surfaces of the posterior median of the processes assigned to

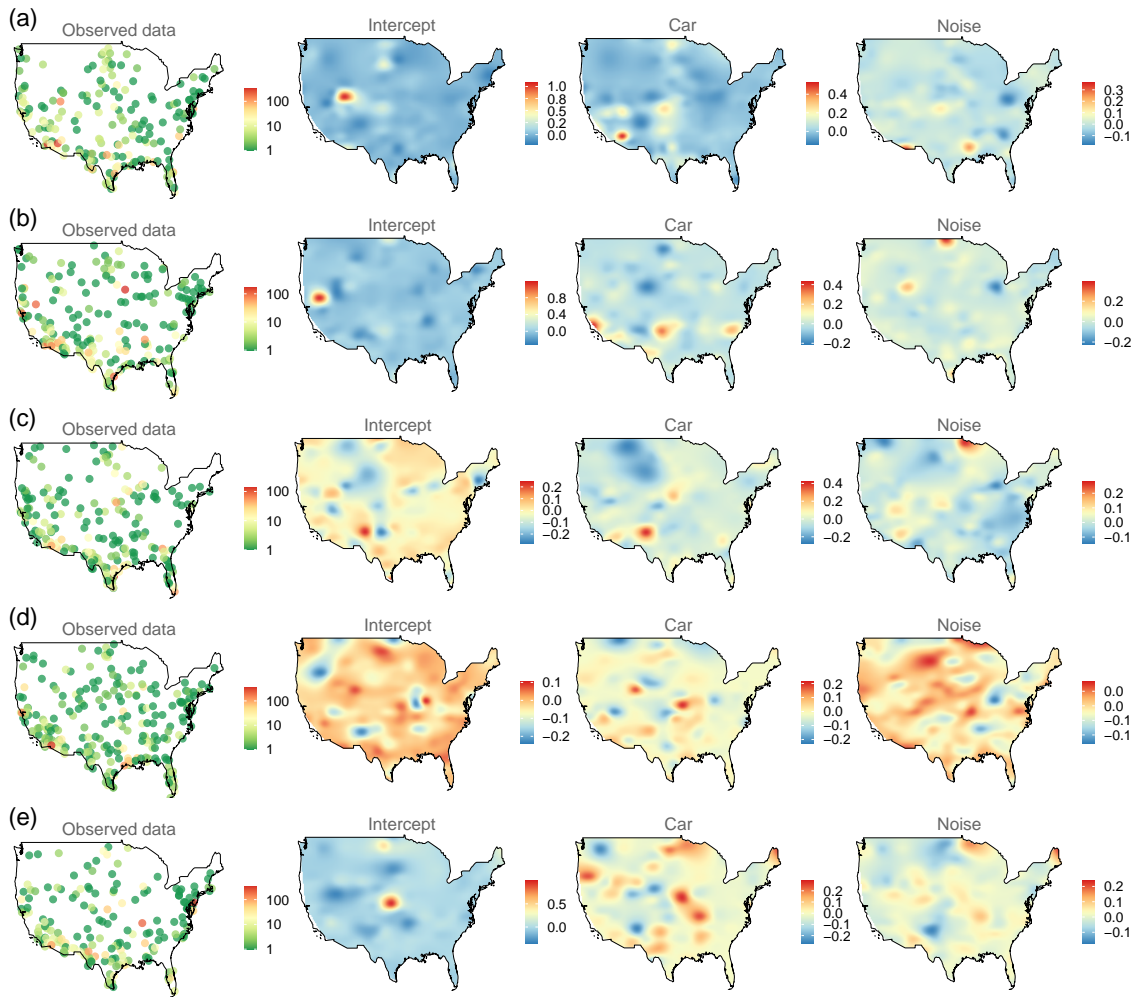


FIGURE A5. (a)–(e) Observed avian point count data and interpolated surfaces of posterior median of spatial-temporal random effects in the intercept as well as slopes of the variables ‘car’ and ‘noise’ for years 2010-2014.

the intercept and the predictors ‘car’ and ‘noise’, revealing clear spatial-temporal patterns in the effect of the predictors.

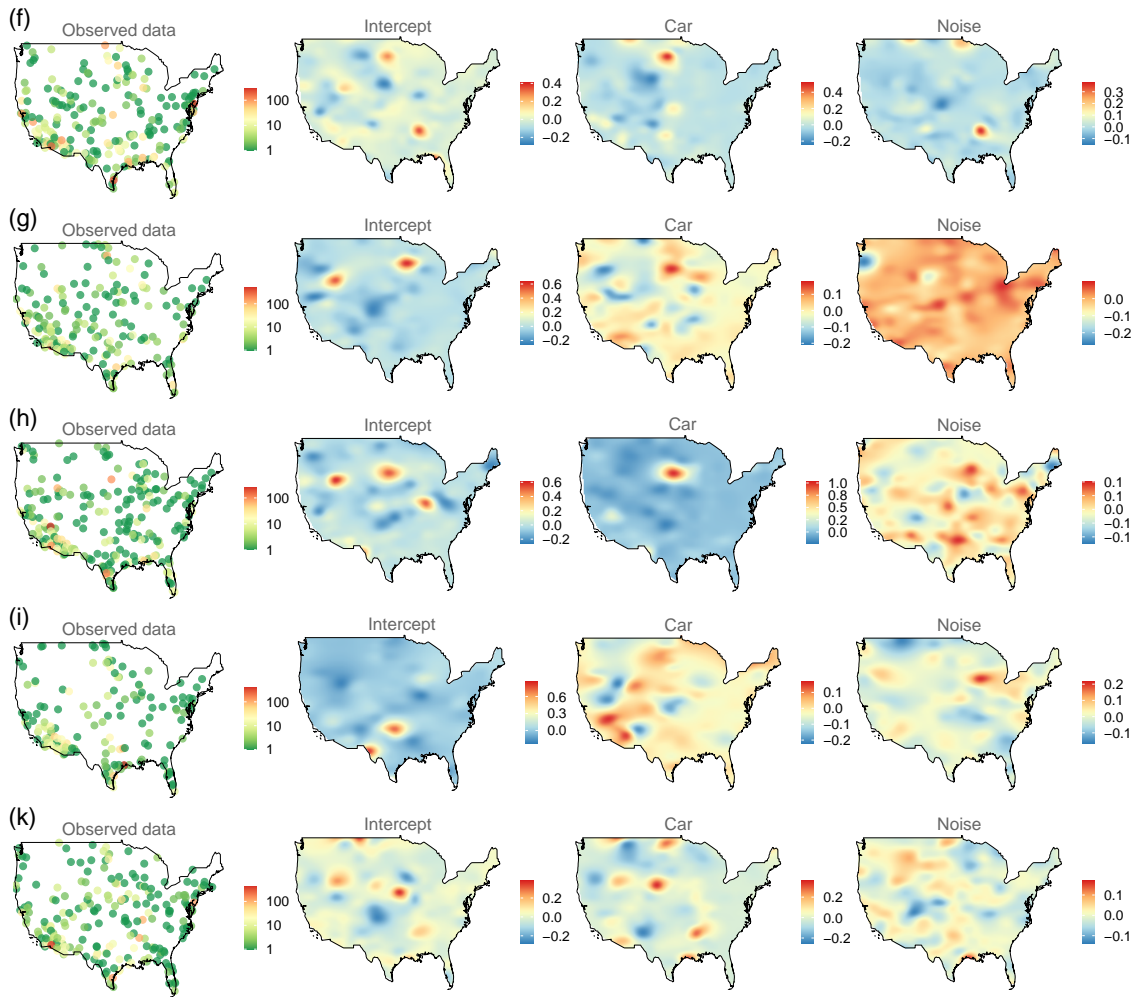


FIGURE A6. (f)–(k) North American Breeding Bird Survey (2015-19): Observed avian point count data and interpolated surfaces of posterior median of spatial-temporal random effects in the intercept as well as slopes of the variables ‘car’ and ‘noise’ for years 2015-2019.